DNA-TR-84-17

URANIUM OXIDE GASEOUS ION AND NEUTRAL INFRARED SPECTROSCOPY

J. Wormhoudt
Aerodyne Research, Inc.
45 Manning Park
Billerica, MA 01821

31 December 1983

Technical Report

CONTRACT No. DNA 001-82-C-0063

THIS WORK WAS SPONSORED BY THE DEFENSE NUCLEAR AGENCY
UNDER RDT&E RMSS CODE B322082466 I25AAXHX00046 H2590D.

Prepared for
Director
DEFENSE NUCLEAR AGENCY
Washington, DC 20305

Destroy this report when it is no longer needed. Do not return to sender.

PLEASE NOTIFY THE DEFENSE NUCLEAR AGENCY, ATTN: STTI, WASHINGTON, DC 20305-1000, IF YOUR ADDRESS IS INCORRECT, IF YOU WISH IT DELETED FROM THE DISTRIBUTION LIST, OR IF THE ADDRESSEE IS NO LONGER EMPLOYED BY YOUR ORGANIZATION.

REPORT DOCUMENTATION PAGE

1a REPORT SECURITY CLASSIFICATION: UNCLASSIFIED	1b RESTRICTIVE MARKINGS: N/A
2a SECURITY CLASSIFICATION AUTHORITY: N/A	3 DISTRIBUTION/AVAILABILITY OF REPORT: Approved for public release; distribution unlimited.
2b DECLASSIFICATION/DOWNGRADING SCHEDULE: N/A since Unclassified	
4 PERFORMING ORGANIZATION REPORT NUMBER(S): ARI-RR-383	5 MONITORING ORGANIZATION REPORT NUMBER(S): DNA-TR-84-17
6a NAME OF PERFORMING ORGANIZATION: Aerodyne Research, Inc. / 6b OFFICE SYMBOL (If applicable):	7a NAME OF MONITORING ORGANIZATION: Defense Nuclear Agency
6c ADDRESS (City, State, and ZIP Code): 45 Manning Park, Billerica, MA 01821-3976	7b ADDRESS (City, State, and ZIP Code): Washington, DC 20305
8a NAME OF FUNDING/SPONSORING ORGANIZATION: Defense Nuclear Agency / 8b OFFICE SYMBOL (If applicable): RAAE	9 PROCUREMENT INSTRUMENT IDENTIFICATION NUMBER: DNA 001-82-C-0063
8c ADDRESS (City, State, and ZIP Code): Washington, DC 20305	10 SOURCE OF FUNDING NUMBERS: PROGRAM ELEMENT NO: 62715H; PROJECT NO: I25AAXH; TASK NO: X00046; WORK UNIT ACCESSION NO: 005910

11 TITLE (Include Security Classification)

URANIUM OXIDE GASEOUS ION AND NUETRAL INFRARED SPECTROSCOPY

12 PERSONAL AUTHOR(S): J. Wormhoudt

13a TYPE OF REPORT	13b TIME COVERED	14 DATE OF REPORT (Year, Month, Day)	15 PAGE COUNT
Final	FROM 820101 TO 831231	1983, December 31	62

16 SUPPLEMENTARY NOTATION

This work was sponsored by the Defense Nuclear Agency under RDT&E RMSS Code B322082466 I25AAXHX00046 H2590D.

17 COSATI CODES		
FIELD	GROUP	SUB-GROUP
20	06	
07	04	

18 SUBJECT TERMS (Continue on reverse if necessary and identify by block number)

Infrared Spectroscopy; Uranium Oxide Ions; Infrared Radiation; Nuclear-Induced Infrared; Uranium Oxides

19 ABSTRACT (Continue on reverse if necessary and identify by block number)

Spectra of gaseous uranium oxide vibrational-rotational bands have never been observed, in part because of the difficulties in vaporizing uranium. Band strengths are needed by the Defnese Nuclear Agency to predict infrared backgrounds as viewed from satellites following atmospheric nuclear bursts. Aerodyne Research, Inc. has developed an apparatus to do these measurements, using multipass diode laser absorption spectroscopy.

The goal of measuring line positions and strengths was not achieved, but the apparatus constructed shows good promise of providing at least some infrared data with only minor modifications. In the apparatus, uranium vaporized by an electron beam is entrained in a carrier gas. It reacts with oxygen in the flow before being carried into the observation region, a multipass or White cell where tunable diode laser infrared absorption by the oxide molecules takes place. Hollow cathode lamp absorption measurements

20 DISTRIBUTION/AVAILABILITY OF ABSTRACT: ☑ UNCLASSIFIED/UNLIMITED ☐ SAME AS RPT ☐ DTIC USERS	21 ABSTRACT SECURITY CLASSIFICATION: UNCLASSIFIED
22a NAME OF RESPONSIBLE INDIVIDUAL: Betty L. Fox	22b TELEPHONE (Include Area Code): 202-325-7042 / 22c OFFICE SYMBOL: DNA/SSTI

DD FORM 1473, 84 MAR — 83 APR edition may be used until exhausted. All other editions are obsolete.

of the uranium vapor density are made at right angles. Variations in oxygen concentration and flow velocity allow large variations in the relative amounts of different uranium oxide species.

Development of the apparatus has progressed to the point of being able to regularly obtain uranium vapor densities in the observation region of up to 5×10^{10} cm^{-3}, with run times of an hour and more. When the oxygen content of the flow is adjusted for maximum UO production, the resulting UO density is predicted to be about 1×10^{10} cm^{-3}. Using the theoretical band strength, this converts to a peak fractional absorption for the strongest lines of 2×10^{-3}. In similar diode laser/multipass cell experiments at Aerodyne Research this has meant a signal-to-noise ratio of about 5. Better uranium densities in the multipass cell can only be achieved through flow system modifications allowing higher pressure flow, or with a higher power electron beam.

SUMMARY

Spectra of gaseous uranium oxide vibrational-rotational bands have never been observed, in part because of the difficulties in vaporizing uranium. Band strengths are needed by the Defense Nuclear Agency to predict infrared backgrounds as viewed from satellites following atmospheric nuclear bursts. Aerodyne Research, Inc., has developed an apparatus to do these measurements, using multipass diode laser absorption spectroscopy.

The goal of measuring line positions and strengths was not achieved, but the apparatus constructed shows good promise of providing at least some infrared data with only minor modifications. In this apparatus, uranium vaporized by an electron beam is entrained in a carrier gas. It reacts with oxygen in the flow before being carried into the observation region, a multipass or White cell where tunable diode laser infrared absorption by the oxide molecules takes place. Hollow cathode lamp absorption measurements of the uranium vapor density are made at right angles. Variations in oxygen concentration and flow velocity allow large variations in the relative amounts of different uranium oxide species.

The work to date has been done at electron beam powers of up to 4.5 kW. The apparatus includes three stages of differential pumping - the flow system at around 1 torr, the gun chamber at 10^{-3} torr, and an intermediate chamber also pumped by a diffusion pump, at about 10^{-2} torr. The beam must be centered on a small water-cooled hole separating the flow and intermediate chambers. Precise focusing is critical, to attain the high temperatures needed for vaporization without depressing the liquid surface so far that the hole produced is unstable. The necessity for a small spot puts a limit on the gas pressure and electron beam path length through the flow system.

Development of the apparatus has progressed to the point of being able to regularly obtain uranium vapor densities in the observation region of up to 5×10^{10} cm $^{-3}$, with run times of an hour and more. When the oxygen content of

the flow is adjusted for maximum UO production, the resulting UO density is predicted to be about 1×10^{10} cm^{-3}. Visible emission from tract quantities of chemiluminescent U and UO is produced under these conditions and used as an indicator of UO production rates. Using the theoretical band strength, this converts to a peak fractional absorption for the strongest lines of 2×10^{-3}. In similar diode laser/multipass cell experiments at Aerodyne Research this has meant a signal-to-noise ratio of about 5. Better uranium densities in the multipass cell can only be achieved through flow system modifications allowing higher pressure flow, or with a higher power electron beam.

PREFACE

This is the Final Report for Contract No. DNA-001-82-C-0063, "Uranium Oxide Gaseous Ion and Neutral Infrared Spectroscopy." This work is sponsored by the Defense Nuclear Agency under RDT&E RMSS Code B322082466 I25AAXHX00046 H2590. It covers the period from January 1, 1982 to December 31, 1983.

Program work was under the supervision of Dr. Joda Wormhoudt, with apparatus construction and operation done by Mr. Spiros Kallelis, and technical advice received from Drs. Charles E. Kolb, Kurt Annen, Alan Stanton, and Mark Zahniser of Aerodyne and G. Sargent Janes of Avco Everett Research Laboratory. The encouragement of the Defense Nuclear Agency contract technical manager, Mr. Peter Lunn, as well as of Lt. Col. W. McKechney and Dr. H.C. Fitz, Jr., of DNA, is gratefully acknowledged.

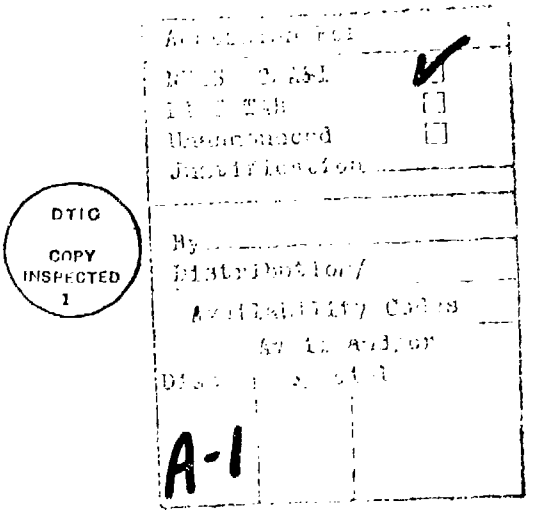

TABLE OF CONTENTS

LIST OF ILLUSTRATIONS

LIST OF TABLES

INTRODUCTION

Infrared Data Requirements

Current uncertainties in the oscillator strengths and spectra of gaseous uranium oxide fundamental vibrational-rotational bands make their accurate determination a high priority in the understanding infrared backgrounds in the 8-14 μm spectral window following atmospheric nuclear bursts. The ionic species, UO_2^+ and UO^+, are of prime importance because they striate along geomagnetic field lines, resulting in a structured background posing particular problems for detection systems associated with infrared sensors. At lower altitudes, the neutrals UO and UO_2 become important terminal products and their radiative characteristics are also required.

Unlike most molecular ions, uranium oxide ions formed in the upper atmosphere are stable against destruction by two body collisions. Because of the low ionization energies and the larger bonding energies for UO and UO_2, the formation of oxide ions by associate ionization processes is exothermic. Dissociative recombination of these ions is in turn endothermic, and they require three body reactions to neutralize their charge. The lifetimes of these ions are thus expected to be very long compared to other ions created by a nuclear event. This opens the possibility of emission from both ions and neutrals due to repeated excitation by sunshine and earthshine. Because of this potentially important source of infrared emission, the infrared spectra and radiative lifetimes of these species must be known in order to predict the overall emission signature in the longwave infrared.[1]

In previous studies, the vibrational spectra of UO, UO_2, and UO_2^+ have been observed in matrix isolation studies carried out at Argonne National Laboratory,[2-4] the National Bureau of Standards,[5,6] and elsewhere.[7,8] The spectrum of UO^+ has never been observed. Additionally, no measurements have been performed of the vibration-rotation spectra of the neutral or ionic uranium oxides in the gas phase, so that precise rotational spacings and

anharmonicity constants are unknown, and no measurements have been made of the f numbers for any of these transitions. Theoretical investigations using multi-configuration self-consistent-field techniques to derive f-numbers are now believed good to within a factor of two. Present estimates of the UO and UO^+ f numbers place both at about 5×10^{-5}, while that for the UO_2^+ ν_3 vibration might be three times that value.[9]

Current knowledge of the vibrational spectroscopy of UO, UO^+, UO_2, and UO_2^+ is summarized in Table 1. The experimental data were obtained by using matrix isolation techniques, in which a shift to lower frequency from the gas-phase value is expected. At the suggestion of Professor R.W. Field of MIT, we applied the observed matrix shift for ThO (thorium is the only actinide element for which gas-phase spectra of the monoxide exist) to the UO matrix value, resulting in an estimated gas-phase ω_e of 836 cm^{-1}. This is the same value resulting from his second suggestion, of adding 20 cm^{-1} to the ω_e for an excited state of ThO (the G state) with the same configuration as ground state UO. This value and the ab initio theoretical prediction of 845 cm^{-1} agree to within their combined uncertainties.

Aerodyne Research, Inc. undertook an experimental program to measure the infrared spectra of gaseous UO, UO^+, UO_2, and UO_2^+ and the absorption oscillator strengths (f numbers) for these transitions. The uranium oxides are made in a flow reactor by reacting uranium atoms in the gas phase with molecular oxygen. Uranium atoms are introduced into the flowing gas stream by electron beam evaporation from the metal, and react with oxygen introduced into the flow stream. The oxides pass through an observation region, a multipass cell which increases the sensitivity to absorption of infrared light from a tunable diode laser.

In the remainder of this section, we will use the above predictions of the molecular radiative properties to estimate the required oxide density in the observation region. In following sections, we will describe in detail the apparatus, its performance to date, and its expected performance with modifications. The original goal of observing infrared spectra of oxides was not achieved in the work reported here. Several unexpected problems resulted

in only arriving at the stage of measuring uranium vapor levels in the observation region which will allow at least marginal infrared absorption experiments. We now consider what level of oxide concentrations are needed.

Table 1. Uranium oxide vibrational spectroscopy.

Molecule	Matrix Center Frequency Observations	Theoretical ω_e Predictions (Ref. 9)
UO	820 cm^{-1}	845 cm^{-1}
UO_2 (ν_3)	776 cm^{-1}	
UO^+		925 cm^{-1}
UO_2^+ (ν_3)	851 cm^{-1}	
UO_3 (ν_1)	745 cm^{-1}	
UO_3 (ν_3)	850 cm^{-1}	

Experimental Sensitivity

In order to determine the molecular number densities required in this experiment, we must first relate the total number of molecules to the number populating the lower state of a given transition. In equilibrium, this number density is given by the product of the electronic, vibration and rotation distribution functions times the total number density. We will now estimate each, for the case of UO. It will be seen that for a 50 m/sec flow rate, the region of high (close to steady-state) UO concentration extends over many centimeters. Assuming complete mixing of the uranium vapor and the column of carrier gas heated by the electron beam with the cold carrier gas, the gas temperature should be less than 500 K. We will see below the collision rate is enough to ensure rotational equilibrium, and probably enough to allow substantial convergence toward vibrational equilibrium as well. The electronic partitioning is less easy to predict, so we will discuss each distribution in turn.

The rotational distribution for a molecule in the Jth rotation level is given by:

$$n_J = n\ (1.44\ B_e/T)\ (2J + 1)\ \{\exp\ [-\ 1.44\ B_e\ J\ (J + 1)/T]\} \quad . \qquad (1)$$

Since the rotational constant for UO is expected to be about 0.33 cm^{-1}, the maximum concentration of UO should be in the j = 17 rotational level. Approximately 2.4% of all UO formed would be in this rotational level.

The partitioning into vibrational levels v_i if vibrational equilibration occurs before the molecule is observed, is given by the Boltzmann factor:

$$x_i = \frac{\exp - (\varepsilon_i/kT)}{\sum_i \exp (- \varepsilon_i/kT)} \qquad (2)$$

where ε_i is the vibrational energy in the ith vibrational level. At 500 K, approximately 0.92, 0.075, 0.006, 0.0004 of all the UO molecules are in the v = 0, 1, 2, and 3 levels, respectively.

The question of electronic equilibrium is complicated by a lack of knowledge of the energy positions of excited electronic states. There are certainly many of them, almost 200, of which on the order of half will be attractive and so have at least a possibility of being quite low-lying. However, the present theoretical calculations indicate no excited electronic states in at least the first 5000 cm^{-1} above the ground state, so their populations will be very small.

The fractional absorption is then related to the absorption cross section (for light whose frequency corresponds to the peak of the absorption line) by the relation

$$\frac{I_o - I}{I_o} = 1 - \exp (- x_i n_J \sigma \ell) \quad , \qquad (3)$$

where I_o is the incident light intensity, I is the intensity transmitted through the flowing gas, $x_i n_J$ is the number density of the absorbing state, σ is the absorption cross section, and ℓ is the length of the light

path through the gas. We may obtain the absorption cross section from the absorption oscillator strength (f number) using the relation

$$\sigma = \frac{\pi e^2 f_{\ell u}}{m_e c \Delta\nu} \left[1 - \exp\left(- h\nu/kT\right)\right] \qquad (4)$$

where m_e is the mass of an electron, c is the speed of light, $\Delta\nu$ is the spectral linewidth, e is the electron charge, h is Planck's constant, ν is the frequency of the light, k is Boltzmann's constant, and T is the temperature.

With the estimates for individual state populations, we can use Eq. (4) to estimate the absorption cross section, and then use Eq. (3) to predict the expected absorption. To do this, we assume a radiative lifetime of 0.04 sec or an f-number of 5×10^{-5}, the present theoretical estimates. This leads to an absorption cross section of 525 $Å^2$ (or a band strength of 1190 cm^{-2} atm^{-1}). Using a single-pass absorption path of 10 cm and the 68 passes achievable with the present multipass system, the expected $(I_o-I)/I$ for a total UO number density of 10^{10} cm^{-3} would be 7×10^{-3}. Figure 1 presents predicted absorption values as a function of radiative lifetime or f number, for a nominal 100 cm path.

Our present lower limit for diode absorption values which allow line strength measurements is about 5×10^{-4}. Thus, it should be possible to produce measurable absorptions with number densities of UO (and perhaps UO^+) in the analysis region of the flow reactor which, as will be documented below, are presently achievable. With only small modifications to the present apparatus, some margin of safety in these observations can be expected. On the other hand, because of differences in their chemistry and the number of hot bands, it will be more difficult to perform similar measurements on UO_2 or UO_2^+, but still possible with more serious system upgrades.

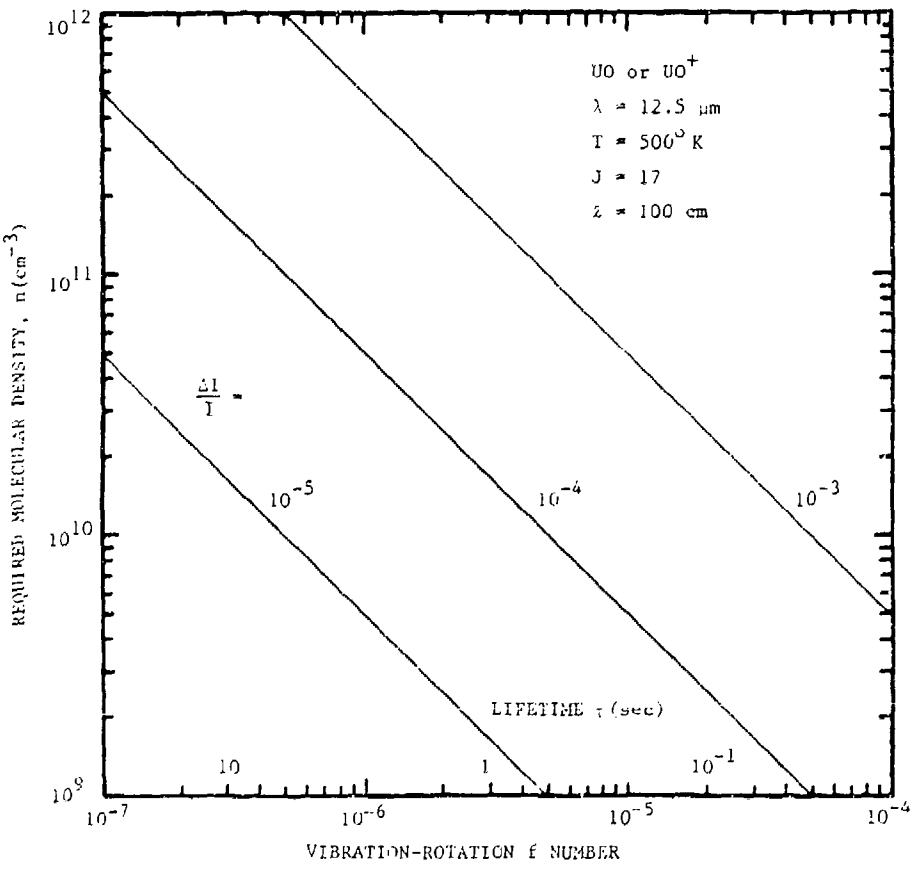

Figure 1. Minimum measurable value of the F number or lifetime as a function of the molecular number density.

The largest source of error in the f number determination will be the estimate of the density n of the absorbing molecules. However, based on absorption measurements of uranium vapor densities and with the present state of knowledge of the kinetics of the reactions of uranium with oxygen, it should be possible to estimate the oxide densities with an uncertainty of on the order of a factor of two. Following sections will discuss both the absorption measurements and the chemical kinetic modeling done to date, after describing the present apparatus. We will then describe planned modifications to achieve even better uranium vapor densities.

APPARATUS DESCRIPTION

Flow System

A schematic diagram of the apparatus is shown in Figure 2, with a perspective drawing of the flow system given in Figure 3. Electron beam evaporation of uranium metal in a water-cooled crucible produces vapor at partial pressures directly over the molten spot of upwards of 10 microns. Argon or helium carrier gas at 0.5 to 2 torr pressure flows past the uranium source and entrains uranium atoms, transporting the mixture along the flow tube. The mixture is warm at the uranium source, but cooling is performed by further mixing with carrier gas. The flux of atomic U produced by this source is directly measured utilizing hollow cathode lamp resonance absorption of well characterized atomic uranium lines. Molecular oxygen can be included in the flow. Variation of conditions allows major concentrations of UO, UO^+, UO_2, and UO_2^+. Detailed discussions of vapor density measurements and the oxide formation chemistry will be given below.

After the desired molecular species are produced in the reacting flow, the infrared diode laser beam traverses the flow. A White cell is used to lengthen the absorption path by producing multiple passes. With good reflecting surfaces more than 60 passes can be obtained, although most previous experiments in our laboratory have used around 40 passes. Several laser diode units might be required, especially if several oxide species were studied, since each unit operates over a narrow spectral range. However, the helium-refrigerated cold head allow mounting of four diodes, and once all are aligned, switching can be routine. The laser line width is up to an order of magnitude narrower than the Doppler widths of the uranium oxide spectral lines. This permits the absorption lines to be easily resolved. The laser beam is passed through a monochromator before entering the White cell, in order to isolate the radiation from an individual laser cavity mode. The laser beam amplitude is modulated using a rotating chopper, and the signal

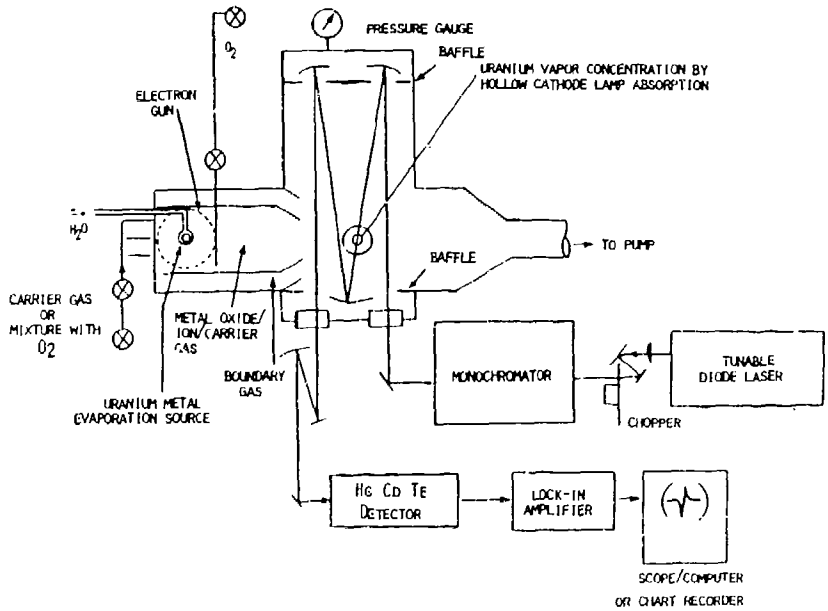

Figure 2. Uranium oxide absorption schematic diagram.

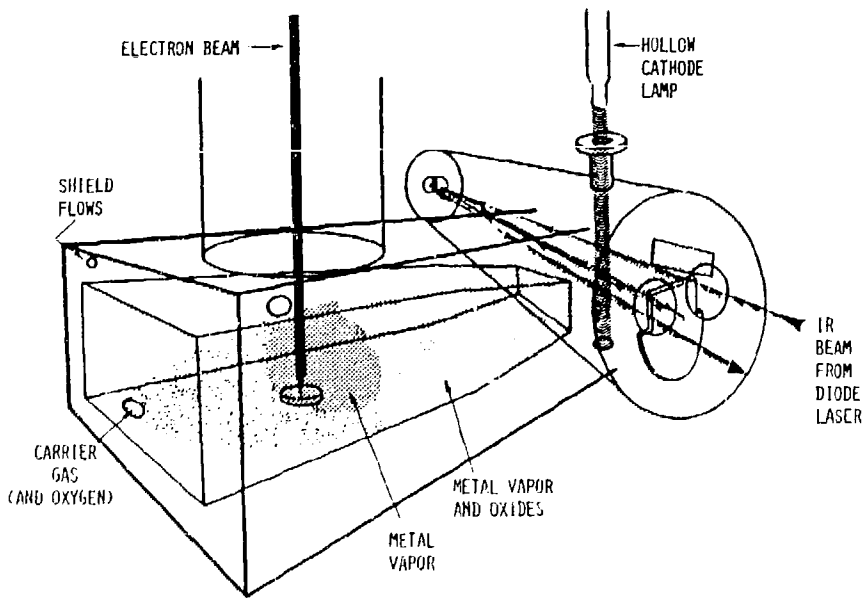

Figure 3. Flow system for infrared spectroscopy of gaseous uranium oxides.

is detected by a liquid helium cooled infrared detector and a lock-in amplifier. The mixture of uranium oxide vapor and carrier gas is trapped in the far end of the test section by a copper wool trap. Because of the extremely low vapor pressure of the refractory oxide, it is easily condensed when coming in contact with room temperature surfaces. By passing through the circulation path of the trap, the metal oxide vapor is removed before the carrier gas reaches the pumps. However, oxide flakes, dust, and metal droplets from the evaporation region can be carried down the flow system and even through the trap, especially during pumpdown.

Carrier gas injected into an external channel was intended to form an aerodynamic window to prevent uranium oxide from depositing on the optics used for the infrared measurements. The flow rate of this shroud flow was to be adjusted so that its velocity matches that of the inner core flow. The core flow, thus confined, would provide an absorption path of 10 cm through the test region. In fact, as will be discussed below, a key to good vapor production is low carrier gas pressure, while a key to good vapor transport is high gas velocity over the source. Therefore, to date the best vapor densities in the observation region have been achieved by putting all carrier gas into the center channel. The baffles indicated in Figure 2 together with purge flows from behind the mirrors will be relied upon to protect their surfaces. In any case, the two channel arrangement allows easy removal of the uranium crucible for loading and cleaning.

The flow velocity is deduced from the measured pressure and flow rate. This velocity is governed by the flow of carrier gas through the system. The primary importance of a high gas velocity will be in overcoming diffusion losses after initial entrainment. These losses are exponential in the flow time, so that at sufficiently high velocities a plateau is reached where further increases give only slight reductions in losses to the walls. Using helium as a carrier gas, we can obtain flow speeds of up to 70 m/sec, which is adequate for this purpose. To maintain this flow speed through flow line and trap means a pumping speed of 300 cfm, where the pump presently in

use with the flow apparatus has an unthrottled capability of at least 1600 cfm.

In addition to reducing diffusion losses, the carrier gas, introduced at 300 K, is used to collisionally cool the uranium oxides formed. Since the flow time is on the order of 3 ms, the uranium oxides will undergo more than 10^4 collisions and should be collisionally cooled, both in rotation and in vibration, to a mixture temperature near that of the carrier gas.

Uranium Source

The source of uranium vapor is a water-cooled crucible containing depleted uranium which is melted by an electron beam. The electron beam is generated by a Pierce-type electron gun originally designed for electron beam welding, shown in Figure 4. This gun has been modified so that it can be differentially pumped to provide sufficient vacuum for electron beam operation as well as allowing high pressure (at present up to 2 torr) in the uranium oxide flow tube source.

The Pierce-type electron gun consists of a cathode heated by a large current supply which in turn floats on a high voltage. The cathode filament, made of tungsten, is thus operated to as high as 30 kV. The cathode to grid voltage is provided by a beam-current sensing power supply. This grid supply provides the desired current level for only the electron gun volume. The actual operating power of the electron beam is then varied by changing the cathode voltage to the anode ground. Although the power supply is nominally capable of 250 mA at 30 kV, arcing problems have limited the voltage obtainable in the 220-240 mA range to 18 to 21 kV, with the maximum power achievable in stable operation being about 4.5 kW. Slightly higher powers have been obtained momentarily, followed by arcing, both internally and at the cable couplings indicated at the top of Figure 4.

Electron beam sources have been operated by Avco Everett Research Laboratories to generate large quantities of uranium vapor. Discussions with G. Sargent Janes of Avco have been very helpful in understanding and improving our apparatus. Their experience helps us to estimate the vapor pressure

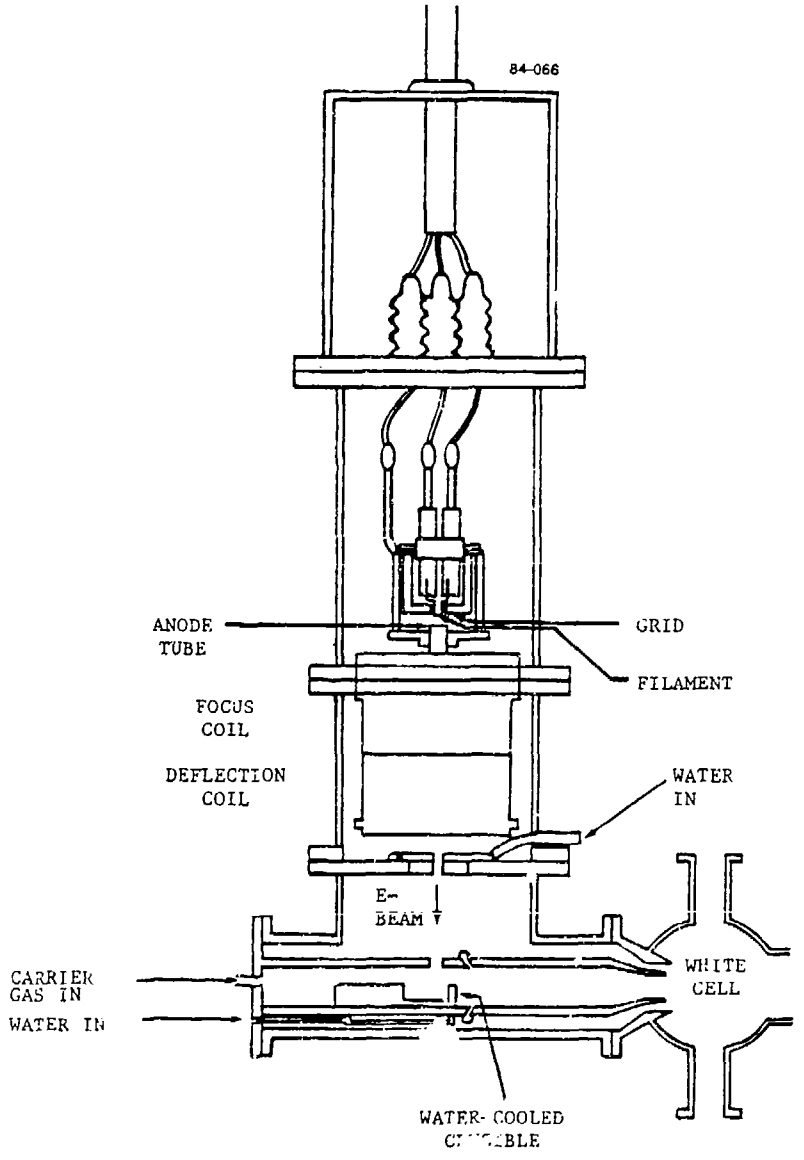

Figure 4. Electron beam evaporation source.

attainable with our system. This requires a heat transfer calculation which yields the temperature of the molten metal, which will be described below. Such a calculation still involves some uncertainties, such as the fraction of the electron beam energy deposited in the uranium before backscattering from the surface (taken to be 0.5), and the thermal conductivities of solid and molten uranium (which increase with temperature). A conservative estimate indicates that temperatures up to 2400 K are quite possible. This temperature would lead to uranium vapor number densities directly over the molten metal of almost 10^{15} cm^{-3}.

Safety Procedures

Like other heavy metal substances, uranium and uranium oxide are poisonous. In addition, uranium metal is pyrophoric. It will spark if its protective oxide coating is broken, and large amounts deposited in vacuum can burst into flame when exposed to air. (Only at the very end of the present work had enough uranium been deposited for this to occur in our apparatus, and then only mildly.) Careful procedures must be followed to prevent inhalation and ingestion as well as laboratory contamination. To identify these procedures, we had discussions with workers at the University of Pittsburgh, the Lawrence Livermore Laboratory, and Avco Everett Research Laboratory, all of whom had been actively involved in long-term programs which use uranium metal vapor. We then retained Murray Bolton of the MIT Radiation Protection Office as a consultant, and working with him designed a set of procedures and safeguards.

These included placement of the apparatus itself inside a hood assembly so that it would be sealed off during loading and cleaning operations. The hood is equipped as a glove box, with gloves used when there is any chance of burning of uranium when the vacuum system is brought up to air. This burning is regarded as routine by workers in the field, but it is a safety hazard because it spreads fine oxide dust, so it is important that it occur while the apparatus is still sealed. (A Metal-X Class D fire extinguisher is placed by the apparatus, but its use has never been necessary.) The hood is equipped

with an exhaust blower so that dust released in cleaning is retained inside it. The blower exhausts through an absolute filter which traps 99.97% of all particles of 0.3 μm diameter and larger. A suction hose can be attached to the blower to act as a vacuum cleaner during apparatus cleaning. A tap off the blower intake pulls air through a filter paper holder which acts as a continuous air monitor, with filters periodically sent to MIT for readings. Filters are also used for wipe tests of the apparatus and laboratory, and occasional urine samples are taken, with all analysis being done at MIT. In addition, ring badges (monitored quarterly) are worn when work is done near significant amounts of uranium. None of these monitoring procedures have indicated exposures even remotely approaching the NRC regulations (which, incidentally, are based not on radiation, but on the lower limits of chemical toxicity). Properly handled, there is no radiation hazard from the small amounts of depleted uranium we use, and the protective oxide coating allows it to be stored and worked in air.

All oxide dust not vacuumed into the absolute filter is collected using wipes which are bagged and retained in a sealed drum for eventual shipment to a disposal site. Apparatus parts which require new machining are cleaned by soaking in nitric acid. The acid can be evaporated, leaving a residue which is bagged for storage. All surfaces can be checked for cleanliness using a Geiger counter, which is more sensitive than visual inspection. The Geiger counter is also necessary to check for x-rays produced by the electron beam, especially upon impact on the uranium. With appropriate lead shielding, our apparatus shows no x-ray leaks.

Uranium Oxide Chemistry

Thermochemical information for the uranium-oxygen system is shown in Table 2. Also presented are reaction rate constants, both those that have been measured and estimates for other key reactions. Due to large exothermicities and favorable electronic and spin correlations, some rates for these reactions are extremely fast even at low temperatures. In addition, the

Table 2. Uranium/oxygen chemistry.

Reaction Number	Reaction	Reaction Rate Constant	Exothermicity (kcal-mole^{-1})
(R1)	$O_2 + U \rightarrow UO + O$	1.1×10^{-10} cm^3-sec^{-1} (10)	62
(R2)	$O_2 + U \rightarrow UO_2^+ + e$	2×10^{-12} cm^3-sec^{-1} (11) 2.5×10^{-12} cm^3-sec^{-1} (12)	117
(R3)	$O_2 + UO \rightarrow UO_2 + O$		47
(R4)	$O_2 + UO_2 \rightarrow UO_3 + O$		-20
(R5)	$O_2 + U^+ \rightarrow UO^+ + O$	8.5×10^{-9} cm^3-sec^{-1} (11) 5.6×10^{-10} cm^3-sec^{-1} (13)	76
(R6)	$O_2 + UO^+ \rightarrow UO_2^+ + O$	2×10^{-9} cm^3-sec^{-1} (14) 1×10^{-9} cm^3-sec^{-1} (13)	50
(R7)	$O + U \rightarrow UO^+ + e$	2.5×10^{-10} cm^3-sec^{-1} (10)	70
(R8)	$O + UO \rightarrow UO_2^+ + e$		55
(R9)	$UO^+ + e + M \rightarrow UO + M$	10^{-26} cm^6-sec^{-1} (15)	110
(R10)	$UO^+ + e + e \rightarrow UO + e$	$3 \times 10^{-8}/T^{4.5}$ cm^6-sec^{-1} (16)	110
(R11)	$UO_2^+ + e + M \rightarrow UO_2 + M$		100
(R12)	$UO_2^+ + e + e \rightarrow UO_2 + e$		100
(R13)	$UO + O_2 \rightarrow UO_2 + O$	5×10^{-11} cm^3 sec^{-1} (est)	57
(R14)	$UO_2 + O_2 \rightarrow UO_3 + O$	5×10^{-11} cm^3 sec^{-1} (est)	21

ion producing reactions are exothermic because of the strong binding energy of uranium to oxygen and the low (~5 eV) ionization potentials to UO^+ and UO_2^+. Therefore, ions are readily formed in reactions at room temperature. Using a triple crossed beam technique, Fite, et al.[10] have shown that the exothermic Reactions 1 and 7 have gas kinetic rate constants. The low ionization potential for UO^+ makes it stable to dissociative recombination,

thus requiring three body recombination to return to the neutral species via Reactions 9 and 10.

The rates quoted for neutral-stabilized recombination,[15] reaction (R9), and electron-stabilized recombination,[16,17] reaction (R10), are based on theories which have been found to be quite successful in describing a variety of plasma data. As the rates are not expected to be very sensitive to the identity of the ions, they should also be good estimates for reactions (R11) and (R12), respectively. Rates (R13) and (R14) are simply assumed parameters. Fast UO_3 formation interferes with the generation of the lower oxide species we wish to study, especially UO_2. Here the rates are assumed equal; if UO_3 formation were faster, other methods of UO_2 production would have to be considered. However, from the exothermicities at least, the assumption of equal rates is a conservative one.

The one-dimensional chemical kinetic option of the Aerodyne PACKAGE code is used to predict concentrations as the reacting mixture travels down the flow tube. All the rates in Table 2, as well as a wall loss (as will be discussed below, at present only about 10^{-3} of the uranium formed at the source is carried into the observation region), are included in the calculation. The loss is modeled as a reaction with the carrier gas (which is always present in great excess) which destroys uranium vapor and oxides at the appropriate rate.

Production of Uranium Oxides

Using the information in Table 2, one can find flow tube conditions under which reaction with molecular oxygen should produce major concentrations of each of the four oxides UO, UO^+, UO_2, and UO_2^+. Examples of possible conditions appropriate to the production of each of the oxides are given in Tables 3, 4, 5, and 6. Each table presents (1) the flow tube gas velocity and temperature (our present understanding of wall losses removes gas velocity as a useful variable - it must always be high), (2) the densities of the

Table 3. Flow conditions needed to study infrared bands of UO.

Flow Tube Temperature: 300 K		
Flow Velocity: 70 m/sec		
Initial Gases and Concentrations:		
Argon:	4×10^{16} cm^{-3}	
Uranium:	5×10^{13} cm^{-3}	1×10^{14}
	(loses to 4×10^{10} at 21 cm)	(to 6×10^{11} at 21 cm)
O_2:	7×10^{12} cm^{-3}	2×10^{13}
Important Chemical Reactions:		
(R1)	$O_2 + U \rightarrow UO + O$	
(R7)	$O + U \rightarrow UO^+ + e$	
(R9, 10)	$UO^+ + e + M \rightarrow UO + M$; $M = N_2$, e	
Oxides of Uranium Produced by Reactions:		
UO =	1×10^{10} cm^{-3}	2×10^{11}
UO^+ =	1.5×10^{9} cm^{-3}	1.5×10^{10}

Table 4. Flow conditions needed to study infrared bands of UO^+.

Flow Tube Velocity 70 m/sec		
Initial Gases and Concentrations:		
Argon:	4×10^{16} cm^{-3}	
Uranium:	1×10^{14} cm^{-3}	
	(losses to 2.5×10^{11} at 21 cm)	
O_2:	1×10^{12} cm^{-3}	4×10^{12} cm^{-3}
Important Chemical Reactions:		
(R1)	$O_2 + U \rightarrow UO + O$	
(R7)	$O + U \rightarrow UO^+ + e$	
Oxides of Uranium Produced by Reactions:		
UO =	7×10^{9} cm^{-3}	2×10^{10} cm^{-3}
UO^+ =	3×10^{9} cm^{-3}	5×10^{9} cm^{-3}

reactants and carrier gas, (3) the dominant reactions for the particular temperature and reactant concentrations, and (4) the concentrations of uranium oxides resulting in the observation region, 21 cm downstream from the vapor source. Figures 5 through 8 present corresponding plots of oxide mole fractions through the flow system from source to observation region.

Table 5. Flow conditions needed to study infrared bands of UO_2.

Flow Tube Velocity: 70 m/sec

Initial Gases and Concentrations:

Nitrogen:	3×10^{16} cm^{-3}
Uranium:	5×10^{13} cm^{-3} (to 5×10^{10} at 21 cm)
O_2:	4.4×10^{13} cm^{-3}

Important Chemical Reactions:

(R1)	$U + O_2 \rightarrow UO + O$
(R3)	$UO + O_2 \rightarrow UO_2 + O$
(R6)	$UO^+ + O_2 \rightarrow UO_2^+ + O$
(R7)	$U + O \rightarrow UO^+ + e$
(R8)	$UO + O \rightarrow UO_2^+ + e$

Oxides of Uranium Produced by Reactions:

UO_2	$= 2 \times 10^{10}$ cm^{-3}
UO_2^+	$= 7 \times 10^{9}$ cm^{-3}
UO_3	$= 3 \times 10^{10}$ cm^{-3}

Table 6. Flow conditions needed to study infrared bands of UO_2^+.

Flow Tube Velocity: 70 m/sec

Initial Gases and Concentrations:

Argon:	4×10^{16} cm^{-3}
Uranium:	4×10^{13} cm^{-3} (to 5×10^{10} at 21 cm)
O_2:	2×10^{13} cm^{-3}

Important Chemical Reactions:

(R1)	$U + O_2 \rightarrow UO + O$	
(R3)	$UO + O_2 \rightarrow UO_2 + O$	
(R4)	$UO_2 + O_2 \rightarrow UO_3 + O$	
(R7)	$U + O \rightarrow UO^+ + e$	
(R8)	$UO + O \rightarrow UO_2^+ + e$	
(R9, 10)	$UO^+ + e + M \rightarrow UO + M;$	$M = N_2, e$
(R11, 12)	$UO_2^+ + e + M \rightarrow UO_2 + M;$	$M = N_2, e$

Oxides of Uranium Produced by Reactions:

UO	$= 4 \times 10^{9}$ cm^{-3}
UO_2	$= 2 \times 10^{10}$ cm^{-3}
UO_2^+	$= 1 \times 10^{10}$ cm^{-3}
UO_3	$= 1 \times 10^{10}$ cm^{-3}

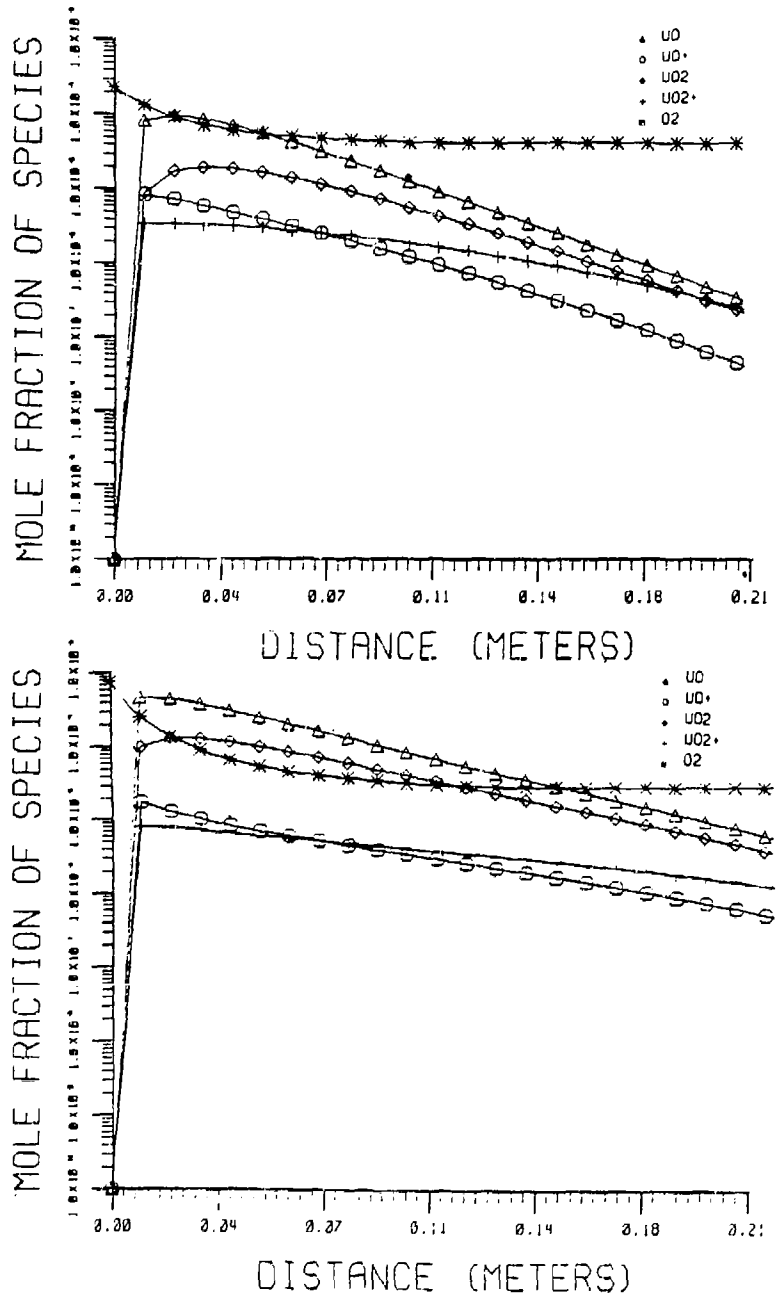

Figure 5. Concentration evolution plots for Table 3 conditions. Upper plot for 5×10^{13} cm^{-3} initial uranium and 10^{-3} losses, lower for 1×10^{14} and 5×10^{-3}.

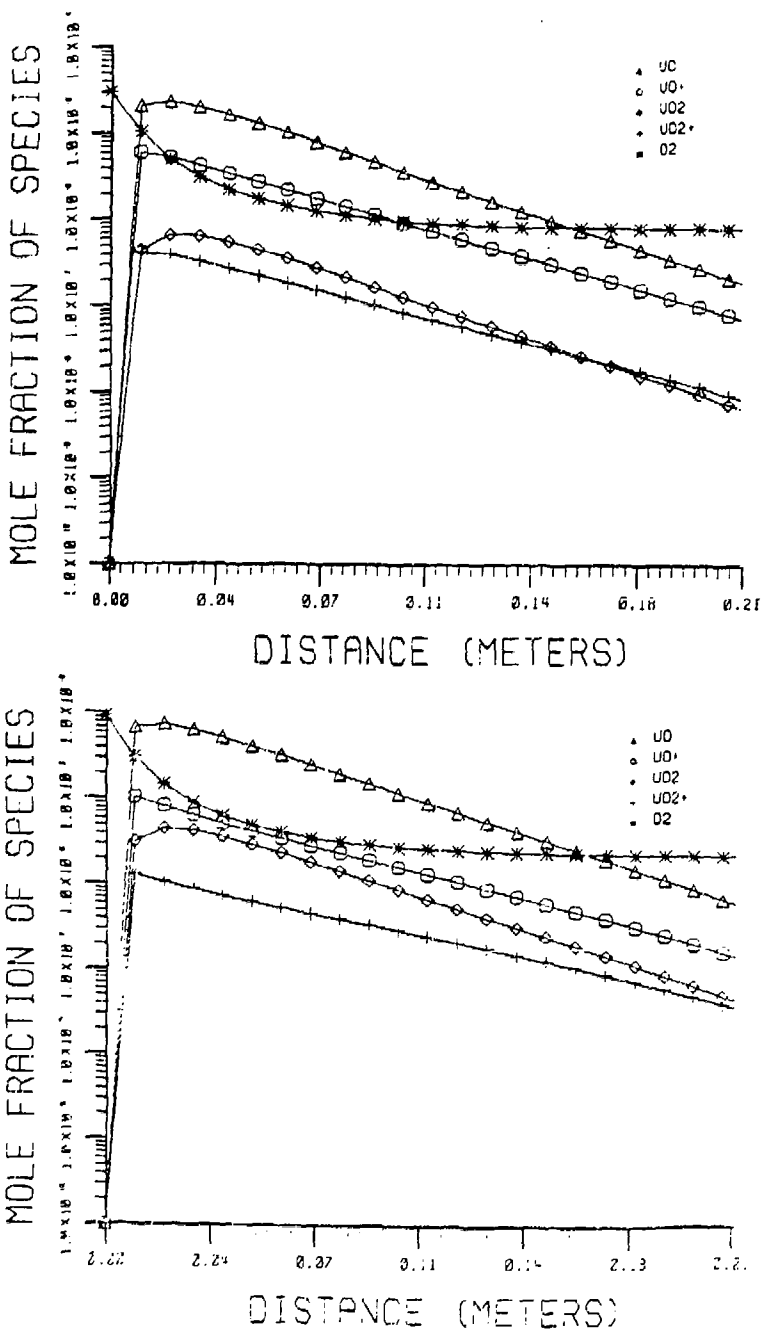

Figure 6. Concentration evolution plots for Table 4 concentrations. Upper plot for 1 x 10^{12} cm^{-3} initial O_2, lower for 4 x 10^{12}.

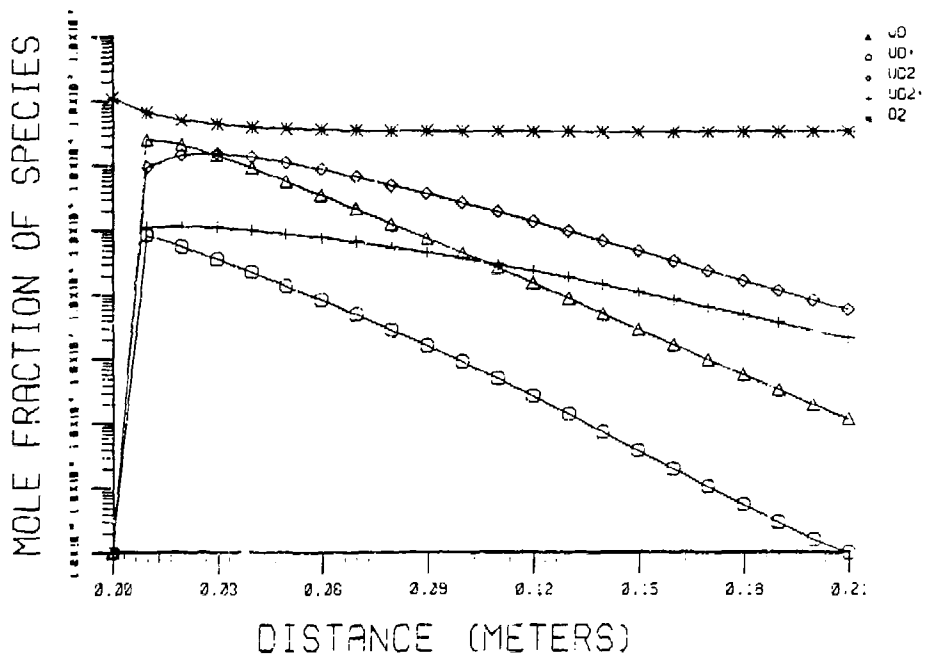

Figure 7. Concentration evolution plots for Table 5 conditions.

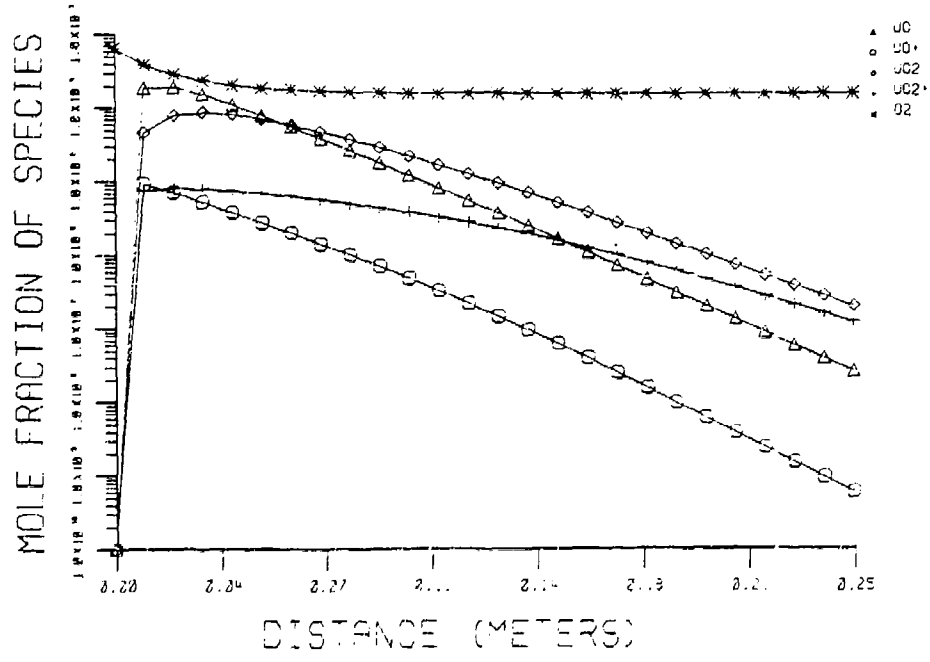

Figure 8. Concentration evolution plots for Table 6 conditions.

Final oxide concentrations show great sensitivity to the initial flow conditions, and the examples presented here are not necessarily optimum conditions. Once a general range of favorable conditions is predicted, it may be easier to peak the desired concentration experimentally.

The dominant reactions and therefore the uranium oxides produced will typically be determined by the choice of reactant densities. For example, in Table 3, for UO production, the dominant reactions are (R1), (R7), (R9), and (R10) because the U atom density is much higher than the O_2 density and because the ion/electron recombination reactions (especially (R10)) are fast at 300 K. The first set of conditions, with a wall loss factor of 10^{-3} leaving 5×10^{10} cm^{-3} uranium in the White cell region if there were no reaction, is believed to be close to those presently obtainable. If losses were reduced by a factor of 5 and uranium production doubled, examples of improvements possible with modifications to be discussed below, the UO concentration is predicted to increase by a factor of 20, as seen in the second entries in Table 3 and the lower part of Figure 5.

In the useful range of the present apparatus, the UO concentration will always exceed that of UO^+. To identify UO^+ lines, it will be necessary to vary the UO^+/UO ratio. To decrease the recombination rates and allow an appreciable steady state concentration of UO^+, the flow temperature could be increased; an increase to 900 K would result in a factor of over 100 decrease in the rate of reaction (R10). However, this would also lower individual line intensities by spreading the population over more levels, so we will instead increase the UO^+/UO ratio by lowering the O_2/U ratio. Unfortunately, this also lowers the absolute UO^+ concentration. In Table 4, adding only 1×10^{12} cm^{-3} O_2 molecules to 1×10^{14} cm^{-3} uranium atoms, the UO^+/UO ratio is about 1/2, while increasing the O_2 by four lowers the ratio to 1/4. Going up by a factor of 20 in O_2 to the conditions of Table 3 lowers the ratio to 1/10. Although these higher O_2 conditions mean UO^+ is the least populous species, its absolute concentration is higher than in Table 4.

To shift the oxides in the White cell to UO_2 and UO_2^+, we must add more O_2. Table 5 and Figure 7 show the results of adding almost as much O_2 as

uranium. Table 6 and Figure 8 show that again, lowering the oxygen favors a higher ion to neutral ratio, although there is still more UO_2 than UO_2^+.

Optical Measurements

The infrared optical train to be used to measure uranium oxide absorption consists of a tunable diode laser, laser beam shaping optics, a mode-selecting monochromator, a multipass absorption cell (White cell), and an HgCdTe detector (see Figure 2). In addition to this optical train, is a second optical train at right angles (Figure 3), consisting of a uranium hollow-cathode lamp, beam shaping optics, a filter or monochromator, and a photomultiplier. The monochromator which is used to receive the hollow cathode lamp radiation can instead take spectra of chemiluminescent emission from the flow. We will discuss each of these optical measurements in turn.

Diode laser scanning is accomplished by changing the diode current in the range of 0 to 2 A. In addition, the tuning region can be displaced by changing the temperature of the helium-refrigerated dewar containing the diode. Although no uranium oxide spectra were attempted, a laser diode was obtained and characterized. The infrared diode we examined covers most of the spectral range between 820 and 920 cm^{-1}. This range would allow measurement of essentially all of the predicted UO vibrational spectrum, assuming it to cover about a 50 cm^{-1} region centered at 845 cm^{-1}. Other similar diodes will allow coverage of the long wavelength infrared regions of interest for other molecules. The diode lases simultaneously in several laser lines, separated by approximately 2 cm^{-1}. A one meter monochromator is thus used to select one laser line at a time. In this way, over 1 cm^{-1} of continuous single mode tuning could be obtained. Figures 9, 10, and 11 show OCS reference gas spectra taken in a region of interest. These spectra are the final step in diode characterization, since they provide accurate emission wavelengths as well as a good indication that single mode selection has been achieved.

The White cell consists of a chamber running perpendicular to the flow tube with mirrors having a 50 cm radius of curvature placed 50 cm apart. Two spherical mirrors with 2 in. diameters are used. The field mirror (at the far

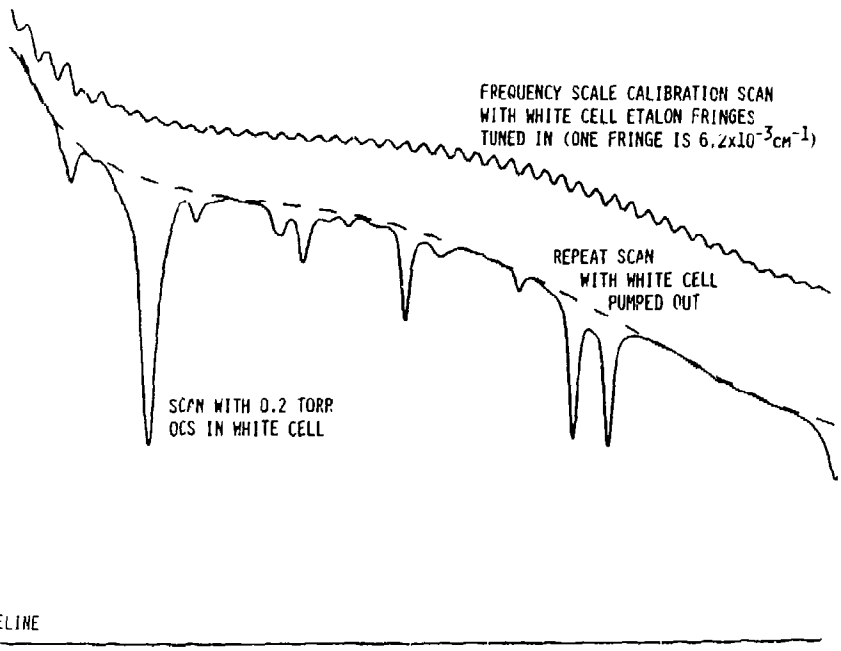

Figure 9. Diode laser spectroscopy - reference gas scan.

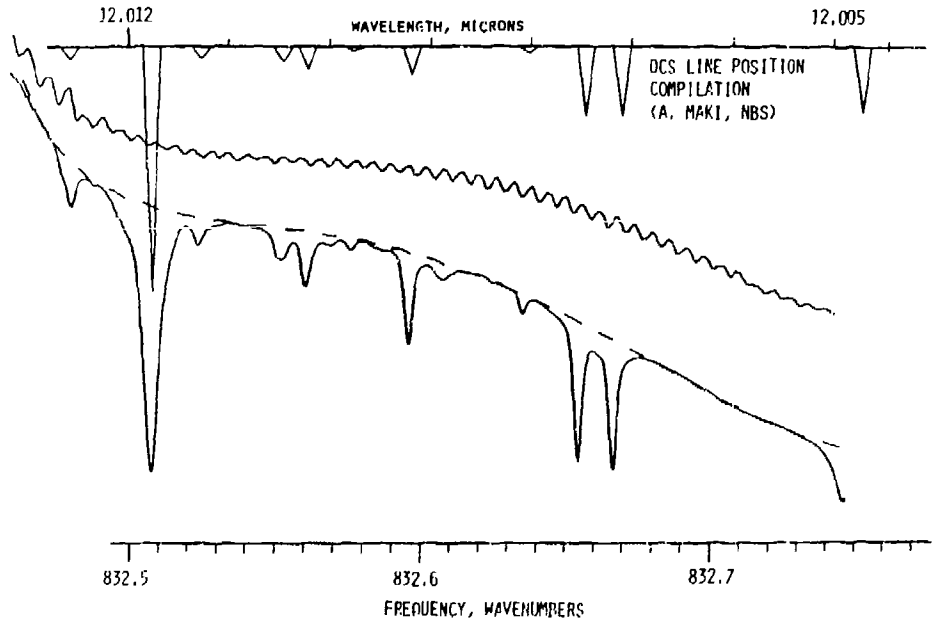

Figure 10. Diode laser spectroscopy - matching reference gas pattern.

end of the cell from the diode laser) is split in the middle, forming two separately adjustable halves. Two slots are cut into the front mirror to allow entrance and exit of the laser beam. The White cell mirrors are gold coated to maximize reflectivity in the 11 μm region. Mirror losses become important when many traversals are made through the test region. When the fractional light loss due to one reflection becomes larger than the extinction of light from an extra pass through the test region, more passes in the White cell would not increase the signal-to-noise ratio. For purposes of observing very small absorption coefficients, this White cell is practically limited to less than 70 passes, resulting in a 1/e drop in the laser intensity due to mirror losses alone.

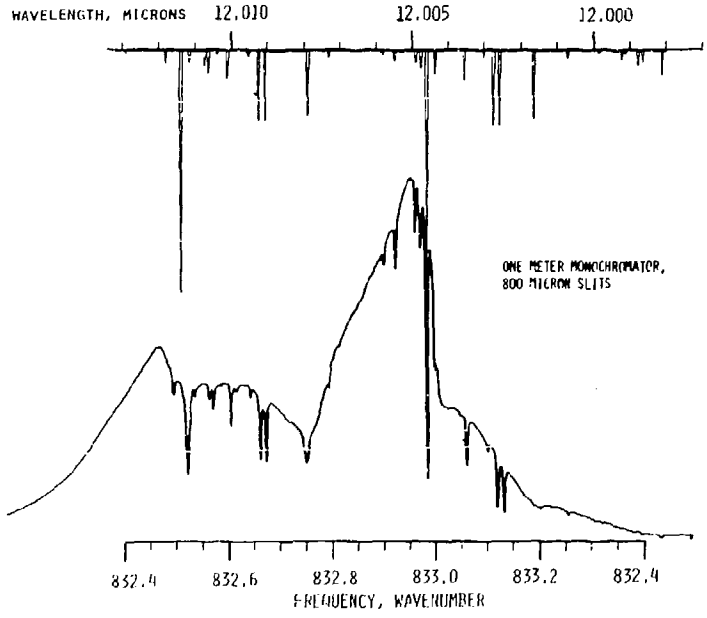

Figure 11. Diode laser spectroscopy - reference gas scan.

As was shown is Figure 3, the hollow cathode light passes through the White cell perpendicular to the flow and infrared beam axes. Quantitative uranium vapor concentration measurements are made using a monochromator to select a single line. The line used in this work was a relatively weak one at

438.7577 nm, with a statistical weight-f number product (gf) value of 0.041. (Wavelength and strength data were obtained from Ref. 20, a very useful line atlas allowing selection of lines with appropriate parameters.) This line was chosen because its useful range (absorptions between, say, 1 and 90 per cent) corresponded to the range of uranium vapor densities expected with the present system.

Concentrations are obtained from the atomic absorption analogs of Eq. (3) and (4). The $\Delta\nu$ value used is the Doppler linewidth, here taken as 0.012 cm^{-1}, corresponding to uranium vapor at 500 K. The emission gf value quoted above must be multiplied by the ratio of the statistical weights of the upper and lower states to be used in the expression for absorption cross section. The path length must also be estimated; we have assumed 3 cm, which seems to be confirmed by the observations of chemiluminescence in the flow which will be described below. Finally, we must correct for the fact that, if the emission line is wider than the absorption line, some light will be transmitted without significant absorption. The apparent absorption of light will be smaller than that which would be predicted by Eq. (3), or, an apparent optical depth from observed values of $-\ln(I/I_o)$ must be multiplied by a correction factor to obtain the true optical depth ($n\sigma\ell$) in Eq. (3). This factor is a function of the ratio of emission and absorption linewidths. Based on more detailed investigations of magnesium hollow cathode lamp emission lines, we assumed this ratio to be 2. (Since the lines are Doppler broadened, this implies a temperature ratio of 4 and an emitting vapor temperature on the order of 2000 K.) Mitchell and Zemansky[21] have tabulated values of this correction factor (which for ratios of 2 are themselves on the order of a factor of 2.)

Using all of the above values, the optical depth at the line peak is 3×10^{11} times the uranium vapor number density in cm^{-3}. Values of fractional absorption, $(I_o-I)/I_o$, up to 0.4 have been observed. (Somewhat higher values have been seen for less than a minute, while slightly lower values have been maintained for many minutes.) With our assumption of a 3 cm path, this absorption value corresponds to a uranium number density of 6.3×10^{10} cm^{-3}.

To isolate the single line described above, a 1 meter monochromator is required. Besides being awkward, it is often needed in other experiments. So, when quantitative accuracy was not required, a bandpass filter was used. Our filter transmitted from 424 to 453 nm, centered at 436 nm. This bandpass includes a number of strong lines, and is therefore considerably more sensitive to low uranium concentrations than the line discussed above.

In addition to correcting for the imperfect overlap due to different linewidths (approximately, due to the varying strengths of the over 300 lines in the filter bandpass), we must also correct for ion lines (present in emission but not in absorption) and for blackbody emission from the hollow cathode lamp. The result of all three corrections is that about half the hollow cathode light passed by the filter will not be absorbed by any uranium vapor concentration. Even with considerable effort in observing our hollow cathode lamp emission spectra to produce correction factors, and a computer program to sum absorption factors for all lines for a given uranium concentration, this filter system is very difficult to calibrate at high absorptions. Comparison of concentrations from an a priori calibration to simultaneous monochromator observations, using a beamsplitter, showed that they agreed to within a factor of two at low concentrations (in the low 10^9 cm^{-3} range), but that at concentrations above a few times $10^{10} cm^{-3}$, the filter is already reading high by an order of magnitude.

Some of the most interesting observations made possible by our new ability to run for long times with high uranium fluxes have been those of fluorescence from uranium species in the White cell. Whenever uranium is evaporated with a carrier gas flow, a blue-white glow is observed emerging from the flow channel and passing through the White cell. Monochromator scans of its spectrum confirm it to be uranium atomic emission.

When oxygen is added to the flow, its color changes to orange-white, the intensity of the uranium lines in the emission spectrum first increases and then decreases, and new spectral features appear, in the same spectral region identified to us by T. Bieniewski of LANL as containing the strongest bands in his absorption spectra of UO. These features first grow and then decrease in

intensity with increasing oxygen concentration, and other, broader features (perhaps due to higher oxides) begin to appear at the higher oxygen levels. Figure 12 shows examples of emission spectra with and without oxygen added. (Some oxygen will always be present in the flow due to the oxide coating the uranium piece.) The oxygen flow giving a maximum in UO concentration before the uranium is converted to other oxides is roughly consistent with our estimates of the uranium density and with our kinetic modeling of the oxide formation chemistry. The points of disappearance of first U emission, the UO emission, with added oxygen are also consistent. Uranium absorption also disappears with added O_2, again at about the expected point. The absolute intensity of the chemiluminescence means it is associated with a minor process. One example, which is consistent with our thermochemical modeling predictions of a uranium dimer to monomer ratio on the order of 10^{-4}, is

$$U_2 + O \rightarrow UO + U$$

in which both products could have enough energy to be chemiluminescent.

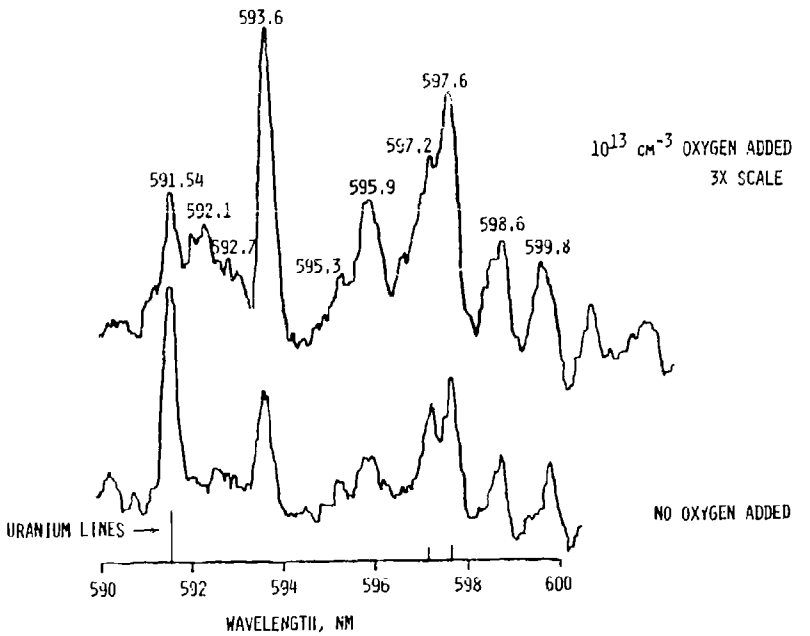

Figure 12. Uranium and uranium oxide visible emission spectra.

APPARATUS PROPERTIES

Much of the contract performance period was taken up with apparatus modification to allow a high enough pressure in the flow system for good vapor transport while still maintaining the necessary vacuum in the gun filament chamber. After improvements to both upper stages of pumping, the remaining point at which progress could be made was the hole separating the flow system and the intermediate chamber, through which the beam must pass. Water cooling eventually allowed a small enough hole (0.15 in. diameter, in a plug 0.5 in. in length) that adequate vapor transport was possible and meaningful data could be taken. For some time, however, observations continued to be plagued by problems with the electron beam drilling through the uranium piece and building up material on the surface, limiting run times and making further progress difficult. Finally, we began to gain some understanding. In this section we discuss what we learned.

Present Status of Experiment

A good deal of work went into investigating the hypotheses that these problems were due to air leaks in the vacuum system, too sharp a focus at the metal, or the wrong composition in the tungsten/uranium mixture. A major breakthrough came with the conclusion, subsequently confirmed by a literature search, that the problems were instead due to reaction of nitrogen with the hot uranium surface, forming uranium nitrides. This makes nitrogen unacceptable as a carrier gas.

Next, we turned to argon as a carrier gas, and quickly learned a second very important lesson. As the carrier gas pressure is increased, diffusion to the walls is reduced; and a larger fraction of the uranium arrives at the detector. However, the vapor density in the White cell did not increase indefinitely with increasing argon pressure in the flow tube, but exhibited a maximum. (This effect had been suspected with nitrogen. However, because of

the difficulties mentioned above, and because its maximum occurred at higher pressure, around the limits of the vacuum system at the time, it was difficult to confirm.) This effect turned out to be due, not to beam energy loss, but to small angle scattering of the electrons, such that at high carrier gas pressures a properly focused spot on the surface of the uranium could not be obtained.

A larger beam spot size eventually lowers the vaporization (an exponential function of temperature) faster than the area is raised. Experiments by R.E. Center[20] on argon and nitrogen in precisely the same pressure and beam voltage ranges make it easy to predict a Gaussian beam diameter for our pressures and path length. This diameter is indeed predicted to become significantly larger over the pressure regime in which the maximum in vapor is observed. It is even possible to reproduce the observation of a maximum using our heat transfer and flow modeling, although predicting the actual pressure value requires some parameters to be substantially different from nominal choices. Therefore our ability to predict uranium temperatures for a given beam power and spot size is not sufficient to allow a priori predictions of where the maximum would occur. The fact that the scattering cross section is proportional to atomic number eventually led us to try helium as a carrier gas. The balance between its scattering cross section (10 times less than argon) and its diffusion cross section (expected to be about four times less) turned out to be optimum for our present system.

Using helium as the carrier gas, the operation of the system and the data we were able to take improved tremendously. We were able to make long runs, of many hours duration, with quite stable uranium vapor fluxes. Uranium vapor densities in the White cell adequate for diagnostic purposes, up to 5×10^{10} cm^{-3}, were easily achievable. This allowed measurement of vapor losses from the evaporation point to the White cell.

Experiment Scaling - Vaporization

The first lesson which can be drawn from those experiments and associated calculations is that the present electron beam system is not powerful enough

to produce the vapor densities required for the full range of desired infrared observations. Predicting what power would be adequate is difficult because of points in the calculations which are difficult to support by any observations using the present system. We will discuss below our heat transfer and vaporization modeling to date. Two considerations limit the improvement in vaporization which can be achieved with a higher power gun. The first is simply the weight loss per unit time which is compatible with long run times in a laboratory-scale apparatus. The second is that while the area which is directly heated by the beam is also limited due to pumping constraints, the temperature of that area cannot be raised indefinitely, because the pressure of vapor leaving the heated spot depresses the liquid below the surface of the bulk metal. Our present weight losses are on the order of 0.1 g/min, and with helium and a tight focus we can observe enough surface depression that it becomes unstable, throwing out sparks of molten metal.

The prediction of how much vapor results from a given power electron beam begins with a heat transfer calculation. The model we used was two-dimensional, with the cylindrical uranium piece being divided into annular radial segments and also into perpendicular axial divisions. This turns the problem into one of a two-dimensional grid of nodes connected by thermal resistances. For conduction within the uranium piece, the resistance between volume elements in the radial direction is given by a conduction only formula,

$$R = \frac{\ln (r_o/r_i)}{2\pi\, kT} \tag{5}$$

where r_o and r_i are inner and outer radii to centers of the two adjoining annuli, k is the thermal conductivity, and t is the axial segment thickness. In the axial direction the resistance is given by

$$R = t/kA_i \quad , \tag{6}$$

where A_i is the area of the ith annular segment in a radial plane.

For heat transfer out of the top and sides of the piece, by radiation only, the resistance is given by

$$R = \frac{T_i - T_w}{\varepsilon\sigma(T_i^4 - T_w^4)} \tag{7}$$

where ε is the emissivity, and σ is the Stefan-Boltzmann constant. For the top the temperature T_w is assumed to be 500 K, while for the sides, which view the water-cooled crucible, T_w is taken as 400 K. Heat transfer out of the bottom is by both radiation and conduction, so the resistance is given by

$$R = \frac{T_i - T_w}{\varepsilon\sigma(T_i^4 - T_w^4) + U_{con}\, A_i (T_i - T_w)} \tag{8}$$

where U_{con} is the contact conductance between the uranium piece and the crucible bottom.

Most of the input parameters for the model have had their values chosen at least in part to bring its predictions closer to observations. For example, ranges for contact conductance values are known for various conditions, but it took observations of heating and cooling rates simply to understand what the contact conditions might be. Again, another parameter is the fraction of electron beam energy which is simply scattered without heating the uranium piece. We were told by Avco Everett that their experience was that this factor was about 0.5, and indeed in our model this value seems to fit our observations as well. The only input which is not based primarily on agreement with observation is the uranium thermal conductivity. We will describe its choice, before turning to our observations and their comparison with the modeling.

A large number of measurements of the thermal conductivity of uranium are available.[23] They cover a temperature range up to within 200 K of the melting point (1406 K). Between this point and room temperature the thermal

conductivity has increased by more than a factor of two. It is expected to continue to increase, and to increase in a different fashion when the uranium becomes liquid. In addition, the experience at Avco Everett was that the heat transfer in liquid uranium was even faster yet than might be extrapolated from the solid, because convection is the major transfer mode. (This led them to several innovations to suppress convection.[24] The last was to mix the uranium with tungsten powder, which both dissolves to raise the liquid viscosity and forms a matrix which retards liquid motion. We also added tungsten powder to our uranium, repeatedly melting regions to mix it in. However, our molten regions are small enough that convection may not yet be a serious problem for us.) We researched the functional behavior of the thermal conductivity with temperature for a number of liquid metals, found that an exponential fit acceptably, and then chose a temperature coefficient in the exponential somewhat above the range of variation to account for the reported fast heat transfer. With all this, the expression adopted for the thermal conductivity in W/m K is

$$K = 30 + 0.02\ (T-773) \quad , \quad T < 1406$$

$$= 30 + 0.02\ (T-773)\ \exp\left[-0.001(T-1406)\right] \ , \ T > 1406 \qquad (9)$$

The parameterization of the model extended all the way from the uranium piece through the crucible to the water-cooled floor of the channel, to which the crucible is attached by screws. A number of different observations were made in order to validate parameter values. For example, both crucible steady state temperatures and cooling rates were measured, using thermocouples, to shed light on the contact conductance between it and the channel. Both types of observations were consistent with the rest of the apparatus being heated by scattered electrons to well above room temperature. (Indeed, the stainless steel outer vacuum wall was observed to reach almost 200 F, with unfortunate

results to be detailed below.) Thus, it acts as a heat source, raising the steady state temperature and slowing the cooling rate when the beam is turned off.

Both crucible heating rates, when the beam is first turned on, and uranium cooling rates after beam turnoff (obtained from color temperatures) can be used to estimate heat transfer out of the uranium. Both types of measurements indicate fast heat transfer, compared to out initial expectations of relative thermal isolation. We modeled this using an emissivity of one, and a contact conductance of 1000 W m^2/K. Conductance values in this range are only plausible if localized melting creates regions of very good contact between the uranium and the copper.

Even with what we believe to be high values, we cannot quite reproduce the observation, that the sides of the uranium piece do not melt although molten spot temperatures are believed to be above 2400 K (justified below). Again, localized melting on the bottom may be a part of the answer. Another part may lie in what at first seems to be yet another contradiction - the time for the top of the uranium piece to be heated to glowing is predicted to be almost twice as long as actually observed. Increasing the uranium thermal conductivity by any reasonable amount does not significantly improve the discrepancy, though it does lower the peak temperature. On the other hand, if the outer layer of the uranium piece were an oxide "skin" which did not conduct well into the bulk metal and therefore was more easily heated by scattered electrons, this might help to reproduce the observation. Then, this same "skin" might allow the sides of the piece to remain rigid, even with the possible localized melting at the bottom.

The present status of the model is that no observation is reproduced quantitatively, which is not surprising considering how difficult it is to characterize the properties of the uranium piece at high temperatures. On the other hand, we feel it is even now useful for extrapolation, for instance for predicting what improvement factor might result from higher beam power. Figure 13 shows temperature contours for the model parameters described above.

The final comparison to be made is between the measured weight loss averaged over a firing (typically 60 minutes or more in length) and the predicted vaporization of uranium atoms. We will base the prediction on the temperature and area of the center segment in the heat transfer model. Other segments do contribute, although typically much less, and in addition the use of a much finer grid might remove some averaging which probably lowers the prediction somewhat, since vaporization is linear in area but exponential in temperature. However, the present calculations using at most 25 radial segments probably have at least the accuracy of the input parameters. With the inputs discussed above, a 4 kW beam (2 kW absorbed) is predicted to heat the central 0.6 diameter region of a 3.2 cm diameter piece to about 2600 K.

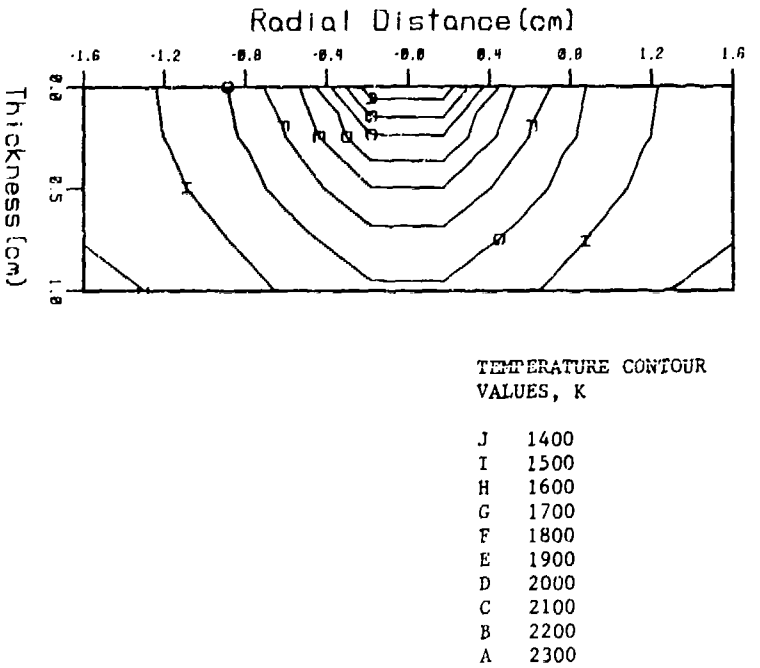

Figure 13. Temperature contours for heat transfer model for 3 kW input power and a uranium contact conductance of 1000 W m^2/K.

To estimate the vaporization rate, we use the vapor pressure formula of Ref. 19, which is plotted in Figure 14, and the gas kinetic effusion formula

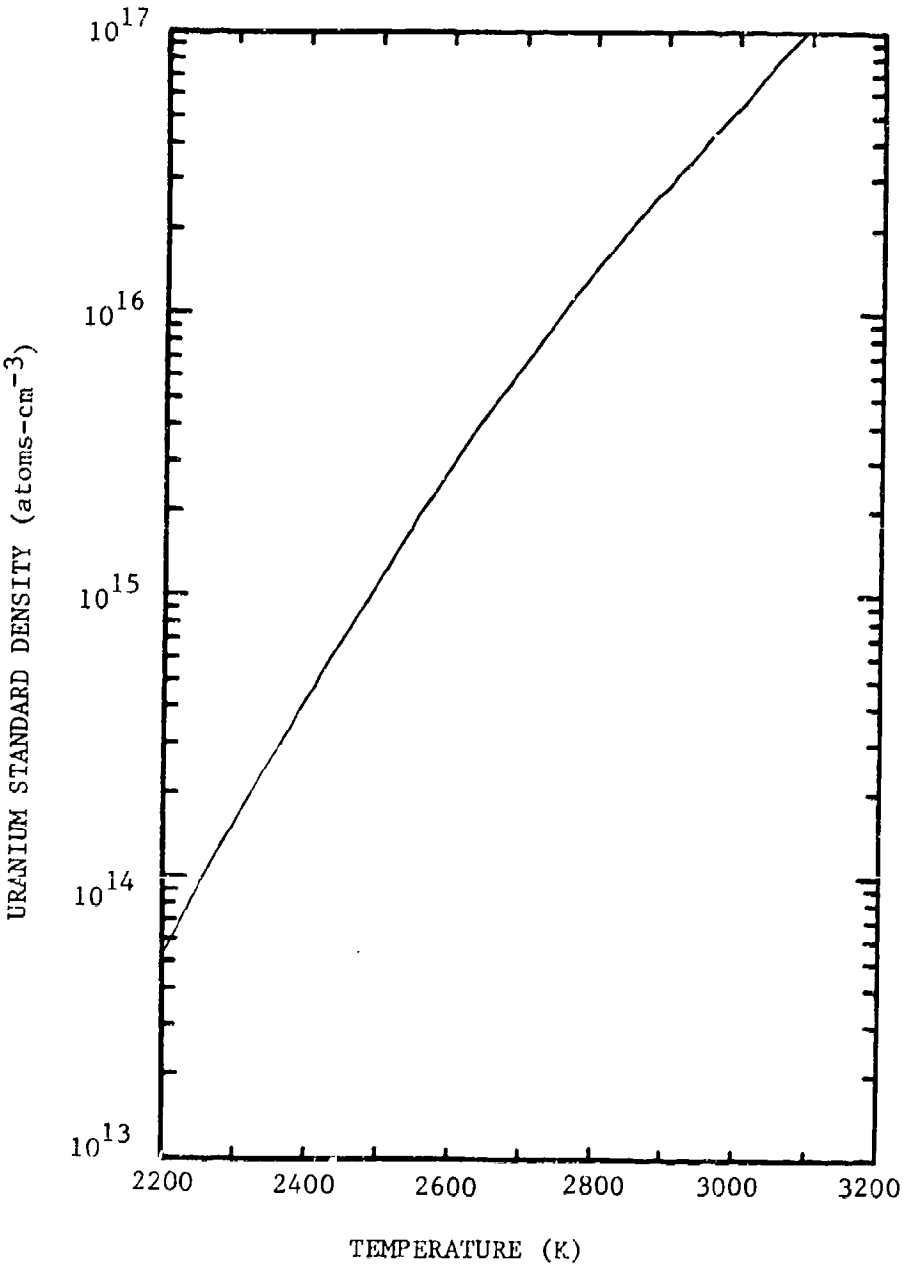

Figure 14. Uranium vapor pressure as a function of temperature.

for molecules per second through a hole (in this case, through a circular area directly above the molten pool),

$$dN/dt = nca/4 \tag{10}$$

In this case, the density n is about 5×10^{14} cm^{-3}, the mean velocity c is 4.7×10^4 cm/sec and the area a is 0.3 cm^2, yielding a vaporization rate of $1.5 \times {}^{18}$ molecules/sec. A typical experimental observation is a weight loss of around 0.1 g/min, or 5×10^{18} molecules/sec. This is by no means perfect agreement, but it is only to be expected given the uncertainty in inputs. Larger beam areas, such as might result from diffusion of the beam at higher carrier gas pressures, result in lower predicted temperatures and a lower vaporization rate.

To produce more vapor than we do at present, we would need to operate at a slightly higher surface temperature, and a much larger heated area, so that the depressed region is stable. Extrapolating the heat transfer and vaporization modeling described above which seem to fit our present observations, we find that an increase in vaporization to 5 g/min would be achieved by raising an area of almost 2 cm^2 to an average temperature of around 3150 K, requiring 30 kW of electron power. That means that the limits of weight loss, beam area, and easily available gun power are all reached essentially simultaneously, with somewhat more than an order of magnitude increase in vaporization. Our experience seems to indicate that a higher power beam will not require a much larger hole separating gun and flow system, with higher differential pumping requirements. Changing the focus point and better water cooling are other options for dealing with larger heat loads.

Experiment Scaling - Vapor Transport

Any additional improvements must be made by increasing the fraction of vapor transported down the flow tube. This is most easily achieved through raising the flow pressure or changing the carrier gas. The pressure is now limited both by defocussing of the electron beam and by the need to keep the

gun at a low pressure when the flow is at a high pressure. A higher power, larger evaporating area system should be less sensitive to small angle scattering, perhaps substantially raising this pressure limit. Vapor densities with argon now peak at under 0.5 torr with argon, compared to above 1 torr for helium, but with similar losses. Again, if a higher power system were less sensitive to defocussing of the beam, perhaps the argon pressure could be increased by a larger factor than that of helium, because the balance of its defocussing and diffusion properties occurs well below the pumping limit of the system.

The total reduction in vapor before it reaches the White cell, determined from weight loss and White cell concentration measurements, is on the order of 10^{-3}. (For example, dividing the 5×10^{18} molecules/sec mentioned before as a typical weight loss by a flow velocity of 70 m/sec and a cross sectional area of about 30 cm^2 gives an initial concentration of 2×10^{13} cm^{-3}, to be compared to typical White cell observations of 2 to 5×10^{10} cm^{-3}.) However, changes in vapor transport with changes in flow pressure or speed are consistent with much smaller diffusion losses to the walls, indicating reductions only on the order of 10^{-1}. These observations give about 750 cm^2/sec for the diffusion coefficient of uranium at about 500 K in 1 torr of helium. This is close to our best a priori guess for the diffusion coefficient. Diffusion losses are exponential in pressure. If they were in the 10^{-3} range, a factor of two increase in pressure would result in a factor of more than 30 increase in vapor transport. However, if we are indeed in the 10^{-1} range, then a pressure increase of two only increases vapor transport by three or less.

One way to understand an additional loss of perhaps two orders of magnitude is to assume that most of the uranium is never entrained, but immediately deposits out on the wall of the flow tube. That is, the evaporating uranium atoms emerge with a directed velocity towards the wall, and only that fraction that undergo enough collisions to be redirected along the flow are in fact entrained. To estimate an attenuation factor, one can multiply the helium collision cross section by both an efficiency factor on

the order of the helium/uranium mass ratio and by a fraction of the total helium whose thermal velocities (much greater than the flow velocity) are at least partially directed down the flow tube. A plausible guess at such a modified cross section does indeed predict that only 1 percent of the total uranium might in fact be entrained.

The problem, given this loss mechanism, is that in this small-attenuation regime the losses decrease only linearly with increasing pressure. Pressure will still be limited by pumping capacity and the size of the hole needed to transmit the beam. It seems that the most we can hope for even with another substantial rebuilding of the vacuum system is about a factor of five increase in vapor transport using helium, or perhaps a factor of ten using argon.

These estimates are based on a detailed analysis of the operation of the vacuum system, which we now proceed to outline. Figure 4 shows the three vacuum chambers. The present 0.15 in. diameter hole separating the flow and intermediate chambers is probably close to the smallest possible. Its construction as a hole in a copper plug which is press-fit into a water-cooled copper plate seems adequate in terms of survival - occasional misalignments gradually widen the hole, but there has been no more melting shut of the hole, which happened several times before water-cooling was installed. Sustained temperatures of above 600 K have been observed by a thermocouple pressed into the hole plug, although with good focus and centering the steady-state temperature for 4 kW beam operation is around 500 K. Further narrowing the hole and raising temperatures would not only bring the edge of the hole uncomfortably close to the melting point of copper (1355 K) but also be in the range of removing a significant fraction of the beam power, so we expect to retain essentially the same hole diameter.

With this hole, 1.6 torr of He in the flow system, close to the practical limit of operation with the present vacuum system, results in an electron gun pressure of about 1×10^{-3} torr. This is at the upper limit of the gun operating range, and is likely to decrease filament lifetimes. (With 1/4 in. and 3/16 in. holes, this limit is reached at about 250 and 500 torr flow pressures, respectively.) Under these limiting conditions, the pressure in

the intermediate chamber is slightly under 0.02 torr. It is this intermediate chamber which is critical, since these conditions also correspond to the throughput limit of its present pump. Therefore, while improving the conductance out of the intermediate chamber will result in a lower pressure for any flow system pressure, the limiting flow system pressure will be the same. However, replacing the diffusion pump will allow significant improvement, based on the following observations of throughput and conductance values.

With 1 torr He in the flow system, we observe an intermediate chamber pressure of about 0.008 torr. Using the formula for the conductance of a tube in the continuum flow regime (6196.5 $\Delta p d^4/\ell$ cfm, where d and ℓ are tube diameter and length in inches, and Δp is the pressure drop across the tube in torr) the predicted conductance for the water-cooled hole is somewhat over 6 cfm. With the rating of the diffusion pump/baffle/gate valve system at 2540 cfm, the predicted conductance out of the intermediate chamber is 420 cfm. It can be seen that these values lead to throughputs (products of conductance and pressure) which differ by almost a factor of two. In fact, throughputs in and out of any chamber must be equal, so we conclude that the actual hole conductance is smaller (the hole is in fact too short a "tube" for the formula to apply exactly), and that the pump and manifold conductance out of the chamber may in fact be larger. A compromise throughput value would then be around 5 torr cfm. This is significant because the rated throughput limit for this pump is 5.3 torr cfm, and it is indeed observed to fail at flow system pressures only slightly above 1 torr.

For the above conditions, the pressure in the gun chamber is about 6×10^{-4} torr. Using the calculated conductance out of this chamber of 250 cfm, throughput matching leads to a conductance between intermediate and gun chambers of about 20 cfm, which is to be expected from the dimensions of the anode tube (through which the beam passes) and the seal between the chamber wall and the gun. Clearly, the throughput for the gun chamber of about 0.15 torr cfm is by no means limiting. The pressure in the gun chamber is only limited by the conductance out of it. However, its manifold is already

6 inch diameter tubing all the way from gun to pump, the same diameter as the chamber itself. Therefore, we do not expect to make improvements in the gun chamber pumping.

The intermediate chamber, on the other hand, has a 2 in. long section of 2 in. diameter pipe. Removing this would more than double the system conductance. With the same pressure in the flow system, this would halve the pressure in the intermediate chamber. Doubling the flow system pressure would double the conductance through the water-cooled hole, thus raising throughput by a factor of four. With a better intermediate manifold this would result in an increase of only two in intermediate and gun chamber pressures, and double the throughput for the intermediate chamber pump. We plan to install a pump with a rated 17 torr cfm throughput limit, thus allowing an increase in flow system pressure of close to this factor of four.

Increasing the pressure will only be beneficial until the limit set by small-angle scattering (about 1.5 torr for He) is reached. A vacuum system which can go beyond this limit will only be useful if the beam path is shortened, or if the gun power is raised to allow heating a larger spot size to the same temperature. We plan to at least halve the path of the electron beam through the high pressure gas. This pressure limit is reached approximately a factor of four lower when argon is the carrier gas, with the absolute loss factor being only somewhat smaller. Therefore, with a substantially higher power beam, argon pressure could be raised to perhaps 2 torr without reaching vacuum system limits, with a smaller loss factor than with the same pressure of helium.

CONCLUSIONS AND PLANNED ADDITIONAL WORK

We entered into this first program with the hope that, if nothing unexpected were encountered, we could obtain spectra for as many as all four molecules of interest. We also acknowledged the possibility that problems could be found which would make any observations with our method impossible. The actual situation turned out to lie between these two extremes. We spent most of the time making modifications to the apparatus, and we learned several important lessons which could only have been learned through operating such an apparatus. In the end, we concluded that the apparatus could indeed provide infrared absorption data, although the probability of success would be raised by some further improvements. In this section, we outline our conclusions.

Synopsis of Current Experiment Status

Our understanding of the electron beam evaporation system has progressed to the point that we can regularly obtain uranium vapor densities in the White cell of about 5×10^{10} cm^{-3}. When the oxygen content of the flow is adjusted for maximum UO production, we believe the resulting UO density should be about 1×10^{10} cm^{-3}. Using the theoretical f-number of 5×10^{-5}, this converts to a peak fractional absorption for the strongest lines of 2×10^{-3}, which in our similar diode laser/multipass cell experiments has meant a signal-to-noise ratio of about 5.

However, our uranium vapor concentration measurement can be in error by a factor of at least two, the f-number prediction has error bounds of a factor of two, and the partitioning among various oxide species could lead to different UO concentrations than is our present understanding. If all of these factors went the wrong way, the actual S/N could be less than one.

Therefore, we recommended that the first task in a continued program be a set of system modifications which hold the promise of improvements in vapor

transport. Then, the second task of achieving good diode laser absorption signal-to-noise and conducting a spectral search for UO lines will, at the very least, provide new knowledge in the form of an upper bound for the line strength. Observation of spectral features would provide an actual band strength measurement along with the first experimental knowledge of vibrational/rotational spectral structure for the gas phase species.

The single system improvement which promises the largest increase in absorption signal is a higher power electron gun, which would allow heating of a larger area of metal to a higher temperature with less sensitivity to diffusion of the beam spot by increasing carrier gas pressure. With a new gun system, a fourth task of continued infrared spectral observations will, if lines were observed earlier, allow flow condition variations, to aid in identifying the species observed and adding new ones. Alternatively, if no lines were observed even with the new gun, the derived upper limit band strength would be far below the present lower limit set by ab initio calculations. In the following subsections, we go on to give some of the details of each of the four planned tasks.

Vacuum System Upgrade

The pressure limit of the flow system, and so its ability to transport vapor, is now set by the maximum throughput of the intermediate stage diffusion pump. Therefore, we will install a new pump which should be able to handle almost double the pressure. We estimate an improvement in vapor transport of a factor between three and four.

The largest part of the task will be to produce a new source section of the flow tube, compatible with the existing electron gun housing and White cell, but incorporating several necessary improvements. The change which will do the most to improve the signal expected in the initial infrared observations is shortening the beam path through the carrier gas. Without this reduction in the beam diffusion, we would not be able to take advantage of the higher pressures possible with a new pump. This is due to electron

beam defocussing which would lower the temperature of the metal leading to a larger decrease in vaporization than the increase in vapor transport.

With the higher power gun, the sensitivity of beam focus to carrier gas pressure will decrease. This would then allow the use of argon as a carrier gas at pressures where it should result in smaller losses to the walls than helium. The gain in vapor transport from this carrier gas switch may well be a factor of five or more. The shortened path length might be very important in achieving this goal, but the effects of defocussing are hard to predict, and with enough beam power a shorter path might no longer be crucial. However, there are several other good reasons why a new version of this part of the apparatus will lead to better operation. These are

- A water cooling jacket is required, since now scattered electrons heat the apparatus to such a degree that o-rings deform, so that cooling after each run results in large leaks,
- An observation window which allows direct viewing of the metal surface would give much better information on how vaporization was proceeding, and
- With a higher power gun, more uranium and a larger crucible will be required, which do not fit in the present apparatus.

Initial Spectral Observations

These spectral observations can begin with the old crucible assembly, so that the performance of the vacuum system improvements may be assessed, and so that all the experience possible may be brought to bear on the design of a new crucible assembly. A larger uranium piece would lead to slightly lower heat transfer and higher vaporizing spot temperatures, even with the existing electron beam system.

The experimental work will be divided between adjusting the optical system for good signal-to-noise, and making infrared absorption measurements. The former involves optimizing optical element placement, minimizing etalon fringes, and eliminating interferences with the laser beam. Infrared measurement runs should begin from the time the apparatus is back together,

since they do not interfere with characterizing any improvements in White cell vapor density brought about by the vacuum system improvements or other work.

Electron Gun Upgrade

The main objective here will be the upgrade of the present electron gun system, now operable only up to beam energies of about 4.5 kW, to a nominal 30 kW system, for which operation well above 20 kW should be routine. Most of the work in this task will be done by the original manufacturer, Nuclide, who in the past year have constructed and shipped two such 30 kW systems. At least a six-month lead time in assembling the power supply is expected. In addition, a new gun will be necessitated by the better water cooling required by higher power operation. Also, a useful improvement to be done at the same time is replacement of the present voltage regulated beam focus and deflection power supplies by current regulated models, which should eliminate our problems with adjusting these settings as the gun heats up and the coil resistances change.

Additional Spectral Observations

The nature of the additional observations will depend on the results of the first set of spectral scans, and on just how much improvement results from the use of a more powerful gun. There are two considerations which limit how large an increase in gun power can be accommodated in a laboratory scale apparatus. The first is simply that the weight of metal evaporated per unit time must be small enough that run times on the order of an hour are possible without recharging. The second results from the fact that, as the vaporization rate is increased by raising the surface temperature of the metal, the liquid surface is pushed down. This depression, which can be calculated, puts a limit on the temperature for a given area before the hole in the liquid becomes physically unstable. The way to maintain stable vaporization is to defocus and increase the beam spot size, but eventually this will also be constrained by the physical dimensions of the apparatus.

Both of these considerations limit possible improvements in vaporization to about an order of magnitude. Our heat transfer calculations predict that this increase could be achieved with the gun system to be obtained. A conservative estimate would be to say that no increase in surface temperature would be attempted, and that the vaporization should increase with the increase in achievable gun power, which we expect will be at least a factor of five. But, the larger area covered by this beam should allow a deeper stable depression, higher surface temperature, and still larger vaporization, by at least an additional factor of two.

With this additional vapor, we will be able to lower detection limits where no lines are seen, observe weaker lines in bands already seen in order to refine spectroscopic parameters, and most importantly, vary the chemistry in the flow to change the relative amounts of the four oxide species, allowing identification of those bands already observed and of new bands associated with different molecules. Thus, even if infrared observations are possible with the present apparatus, the suggested changes are required to meet all the goals of the program.

REFERENCES

1. D.H. Archer, "Requirements for Improved Infrared Prediction Capability: LWIR," Defense Nuclear Agency Report DNA 5471, October 1980.

2. S.D. Gabelnick, G.T. Reedy, and M.G. Chasanov, J. Chem. Phys. 58, 4468-75 (1973).

3. S.D. Gabelnick, G.T. Reedy, and M.G. Chasanov, Chem. Phys. Lett. 19, 90 (1973).

4. D.W. Green, S.D. Gabelnick, and G.T. Reedy, J. Chem. Phys. 64, 1697 (1976).

5. S. Abramowitz, N. Acquista, and K.R. Thompson, J. Phys. Chem. 75, (1971) 2283.

6. S. Abramowitz and N. Acquista, J. Phys. Chem. 76, (1972) 647.

7. H.J. Leary, Jr., T.A. Rooney, E.D. Cater, and H.B. Friedrich, High Temp. Sci. 3, (1971) 433.

8. D.H.W. Carstens, D.M. Gruen, and J.F. Kozlowski, High Temp. Sci. 4, 436 (1972).

9. a) M.J. Krauss and W.J. Stevens, Chem. Phys. Lett. 99, 417 (1983).
   b) H.H. Michels, presentation at DNA IR Data Review Meeting, AFGL, 22 September 1983.

10. W.L. Fite, H.H. Lo, and P. Irving, J. Chem. Phys. 60, 1236 (1974).

11. R. Johnsen and M.A. Biondi, J. Chem. Phys. 57, 1975 (1972).

12. J.C. Halle, H.H. Lo, and W.L. Fite, J. Chem. Phys. 73, 5681 (1980).

13. P.B. Armentrout and J.L. Beauchamp, Chem. Phys. 50, 21 (1980).

14. W.L. Fite and Hsi Hu Lo, "Reactions of UO^+ With Atmospheric Gases," AFGL TR-77-0029 (1977).

15. H.S.W. Massey and E.H.S. Burhop, 1952, "Electronic and Ionic Impact Phenomena," Oxford University Press, New York.

16. E. Hinnov and J.G. Hirschberg, 1962, Phys. Rev. 125, 795.

17. D.R. Bates and A. Dalgarno, 1962, "Electronic Recombination," Atomic and Molecular Processes, D.R. Bates (Ed.), Academic, New York.

18. V. Yousefian, M.H. Weinberg, and R. Haimes, "PACKAGE: A Computer Program for the Calculation of Partial Chemical Equilibrium/Partial Chemical Rate Controlled Composition of Multiphased Mixtures Under One Dimensional Steady Flow," Report No. ARI-RR-177, Aerodyne Research, Inc., February 1980.

19. R.J. Ackermann and G. Rauh, J. Phys. Chem. 73, 769 (1969).

20. R.E. Center, Phys. Fluids 13, 79 (1976).

21. B.A. Palmer, R.A. Keller, and R. Engleman, Jr., "An Atlas of Uranium Emission Intensities in a Hollow Cathode Discharge," Los Alamos Scientific Laboratory Informal Report LA-8251-MS, July 1980.

22. A.C.G. Mitchell and M.W. Zemansky, Resonance Radiation and Excited Atoms, Cambridge University Press, 1971.

23. Y.S. Touloukian, R.W. Powel, C.Y. Ho, and P.G. Klemens, "Thermal Conductivity of Nonmetallic Solids," Thermophysical Properties of Matter, Vol. 2, New York, 1971.

24. a. G.S. Janes, "Flowing Convection Barrier for Evaporation Source," U.S. Patent 3,996,469, Dec. 7, 1976.

    b. K.D. Kennedy, "Mixed Phase Evaporation Source," U.S. Patent 4,035,574, July 12, 1977.

DISTRIBUTION LIST

DEPARTMENT OF DEFENSE

Assistant to the Secretary of Defense
Atomic Energy
ATTN: Executive Assistant

Defense Nuclear Agency
ATTN: RAAE, H. Fitz, Jr
ATTN: RAAE, P. Lunn
ATTN: RAAE, T. Walsh
ATTN: RAAE, K. Schwartz
4 cy ATTN: STTI-CA

Defense Tech Info Ctr
12 cy ATTN: DD

Field Command
DNA, Det 1
Lawrence Livermore National Lab
ATTN: FC-1

Field Command
Defense Nuclear Agency
ATTN: FCPR
ATTN: FCTT
ATTN: FCTT, W. Summa

Joint Strat Tgt Planning Staff
ATTN: JLKS

Under Secy of Def for Rsch & Engrg
ATTN: Defensive Systems
ATTN: Strat & Space Sys (OS)
ATTN: Strat & Theater Nuc for B. Stephan

DEPARTMENT OF THE ARMY

Atmospheric Sciences Lab
3 cy ATTN: DELAS-EO, F. Niles

BMD Advanced Technology Ctr
ATTN: ATC-O, W. Davies
ATTN: ATC-T, M. Capps

BMD Systems Command
2 cy ATTN: BMDSC-HW

Dep Ch of Staff for Rsch, Dev & Acq
ATTN: DAMA-CSS-N

Harry Diamond Labs
2 cy ATTN: DELHD-NW-P

U.S. Army Ballistic Rsch Labs
ATTN: DRDAR-BLA-S, Tech Library
ATTN: DRDAR-BLB, J. Meszaros

U.S. Army Combat Surv & Target Acq Lab
ATTN: DELCS-K, S. Kronenberg

U.S. Army Foreign Science & Tech Ctr
ATTN: DRXST-SD

U.S. Army Nuclear & Chemical Agency
ATTN: Library

DEPARTMENT OF THE ARMY (Continued)

US Army Rsch Office
ATTN: R. Mace

DEPARTMENT OF THE NAVY

Naval Electronic Systems Command
ATTN: PME 117-20

Naval Intelligence Support Ctr
ATTN: Doc Con

Naval Postgraduate School
ATTN: Code 1424, Library

Naval Research Lab
ATTN: Code 2000, J. Brown
ATTN: Code 2627, Tech Library
ATTN: Code 4128.2, J. Johnson
ATTN: Code 4139, D. McNutt
ATTN: Code 4700, W. Ali
ATTN: Code 4700, S. Ossakow
ATTN: Code 4720, J. Davis
ATTN: Code 4780, D. Strobel
ATTN: Code 6700, T. Coffey
ATTN: Code 6780, J. Fedder

Naval Surface Weapons Ctr
ATTN: Code F31
ATTN: Code X211, Tech Library

DEPARTMENT OF THE AIR FORCE

Air Force Geophysics Lab
ATTN: LSP, D. Smith
2 cy ATTN: LKD, R. Narcisi
2 cy ATTN: LKO, R. Huffman
2 cy ATTN: LS, R. Murphy
2 cy ATTN: LSI, P. Armstrong
2 cy ATTN: LSI, R. Sharma
2 cy ATTN: LSP, R. Nadile
2 cy ATTN: LYD, K. Champion
2 cy ATTN: OPR, D. Paulson
4 cy ATTN: CA, A. Stair

Air Force Ofc of Scientific Rsch
ATTN: AFOSR/NC
ATTN: AFOSR/NP

Headquarters
Air Force Systems Command
ATTN: DLAC
ATTN: DLS
ATTN: DLTW
ATTN: DLXP
ATTN: SDR

Air Force Tech Applications Ctr
ATTN: TD
ATTN: Tech Library
ATTN: TT

Air Force Weapons Lab
ATTN: SUL

DEPARTMENT OF THE AIR FORCE (Continued)

Air University Library
ATTN: AUL-LSE

Deputy Chief of Staff
Rsch, Dev, & Acq
3 cy ATTN: AFRDS, Space Sys & C3 Dir

Rome Air Development Ctr
ATTN: OCD, J. Simons

Space Div
ATTN: WE
ATTN: YGD
ATTN: YN

Strategic Air Command
ATTN: ADWA
ATTN: DOTN
ATTN: INCR
ATTN: NRI/STINFO, Library
ATTN: XPFR
ATTN: XPFS

DEPARTMENT OF ENERGY

Department of Energy
Office of Military Application
ATTN: OMA, DP-22

OTHER GOVERNMENT AGENCIES

Central Intelligence Agency
ATTN: OSWR/NED

Department of Commerce
National Bureau of Standards
ATTN: A. Phelps

Department of Commerce
National Bureau of Standards
ATTN: Sec Ofc for J. Devoe
ATTN: Sec Ofc for M. Krauss
ATTN: Sec Ofc for R. Levine
ATTN: Sec Ofc for S. Abramowitz

Department of Commerce
National Oceanic & Atmospheric Admin
3 cy ATTN: F. Ferguson
3 cy ATTN: F. Fehsenfeld

Institute for Telecommunications Sciences
ATTN: G. Falcon
ATTN: W. Utlaut

NASA
ATTN: Code 6801, A. Tempkin
ATTN: Code 900, J. Siry
ATTN: Tech Library
3 cy ATTN: A. Aikin

NASA
ATTN: J. Watts
ATTN: N. Stone
ATTN: W. Roberts

NASA
ATTN: N-245-3, R. Whitten

OTHER GOVERNMENT AGENCIES (Continued)

NASA
ATTN: J. Gray

NASA Headquarters
ATTN: 1 Schardt, Code EE

DIRECTORY OF OTHERS

Government Publications Library-M
ATTN: J. Winkler

Yale University
ATTN: Engrg Department

DEPARTMENT OF ENERGY CONTRACTORS

University of California
Lawrence Livermore National Lab
ATTN: L-10, A. Grossman
ATTN: L-10, H. Kruger
ATTN: L-262, D. Wuebbles
ATTN: L-325, G. Haugan
ATTN: L-48, E. Woodward
ATTN: L-71, J. Chang

Los Alamos National Lab
ATTN: D. Sappenfield
ATTN: G. Smith
ATTN: J. Hopkins
ATTN: Librarian
ATTN: M. Pongratz
ATTN: M. Sandford
ATTN: MS362, Library
ATTN: R. Jeffries
ATTN: T. Bieniewski
ATTN. T. Kunkle, ESS-5

Sandia National Labs
ATTN: T. Cook

Sandia National Labs
ATTN: L. Anderson
ATTN: M. Kramm
ATTN: Org 1250, W. Brown
ATTN: Tech Library, 3141

DEPARTMENT OF DEFENSE CONTRACTORS

Aero-Chem Research Labs, Inc
ATTN: A. Fontijn

Aerodyne Research, Inc
ATTN: C. Kolb
ATTN: M. Camac
ATTN: M. Zahniser
2 cy ATTN: J. Wormhoudt

Aerospace Corp
ATTN: H. Mayer
ATTN: I. Garfunkel
ATTN. J. Reinheimer
ATTN: J. Straus
ATTN: N. Cohen
ATTN: V. Josephson

DEPARTMENT OF DEFENSE CONTRACTORS (Continued)

AVCO Everitt Research Lab, Inc
ATTN: A830
ATTN: C. Von Rosenberg, Jr
ATTN: Tech Library

Battelle Memorial Institute
ATTN: H. Lamuth
ATTN: R. Thatcher
ATTN: STOIAC

Berkeley Rsch Associates, Inc
ATTN: J. Workman
ATTN: S. Bracht

Boston College
ATTN: E. Hegblom
ATTN: W. Grieder

The Trustees of Boston College
2 cy ATTN: Chairman Dept of Chemistry
2 cy ATTN: Chairman Dept of Physics

University of California at Riverside
ATTN: J. Pitts, Jr

California Institute of Technology
ATTN: J. Ajello

Calspan Corp
ATTN: C. Treanor
ATTN: J. Grace
ATTN: M. Dunn
ATTN: W. Wurster

University of Colorado
ATTN: C. Lineberger-JILA
ATTN: G. Lawrence-LASP

Computer Sciences Corp
ATTN: F. Eisenbarth

Concord Sciences Corp
ATTN: E. Sutton

Cornell University
ATTN: M. Kelly

University of Denver
ATTN: D. Murcray

University of Denver
ATTN: B. Van Zyl

Environmental Rsch Inst of Michigan
ATTN: IRIA, Library

EOS Technologies, Inc
ATTN: B. Gabbard

General Electric Co
ATTN: P. Zavitsanos
ATTN: R. Edsall

Geo Ctrs. Inc
ATTN: E. Marram

HSS, Inc
ATTN: M. Shuler

DEPARTMENT OF DEFENSE CONTRACTORS (Continued)

Institute for Defense Anaylses
ATTN: E. Bauer
ATTN: H. Wolfhard

IRT Corp
ATTN: H. Mitchell

JAYCOR
ATTN: H. Dickinson

Kaman Sciences Corp
ATTN: E. Conrad

Kaman Tempo
ATTN: B. Gambill
5 cy ATTN: DASIAC

Kaman Tempo
ATTN: DASIAC

Lockheed Missiles & Space Co, Inc
ATTN: B. McCormac
ATTN: J. Cladis
ATTN: J. Kumer
ATTN: J. Perez
ATTN: J. Reagan
ATTN: M. Walt
ATTN: R. Sears

Mission Research Corp
ATTN: D. Archer
ATTN: D. Sowle
ATTN: F. Guigliano
ATTN: M. Scheibe
ATTN: P. Fischer
ATTN: R. Hendrick
ATTN: R. Kilb
2 cy ATTN: Tech Library

Nichols Research Corp, Inc
ATTN: R. Burns

Pacific-Sierra Research Corp
ATTN: H. Brode, Chairman SAGE

Photometrics, Inc
ATTN: I. Kofsky

Physical Dynamics, Inc
ATTN: A. Thompson

Physical Research, Inc
ATTN: T. Stephens

Physical Research, Inc
ATTN: J. Devore

Physical Science Lab
ATTN: W. Berning

Physical Sciences, Inc
ATTN: D. Green
ATTN: G. Caledonia
ATTN: K. Wray
ATTN: R. Taylor
ATTN: T. Rawlings

Physics International Co
ATTN: Tech Library

DEPARTMENT OF DEFENSE CONTRACTORS (Continued)

Univ of the Commonwealth, Pittsburgh
ATTN: F. Kaufman
ATTN: M. Biondi
ATTN: W. Fite

Princeton University
ATTN: Librarian

R&D Associates
ATTN: F. Gilmore
ATTN: H. Ory
ATTN: R. Lindgren
ATTN: R. Turco
ATTN: P. Haas

R&D Associates
ATTN: B. Yoon
ATTN: J. Rosengren

Rand Corp
ATTN: C. Crain
ATTN: P. Davis

Rand Corp
ATTN: B. Bennett

Science Applications Intl Corp
ATTN: E. Hyman

Science Applications, Inc
ATTN: D. Hamlin
ATTN: D. Sachs

Space Data
ATTN: S. Fisher

SRI International
ATTN: D. McDaniels
ATTN: J. Casper
ATTN: R. Leadabrand
ATTN: W. Chesnut

DEPARTMENT OF DEFENSE CONTRACTORS (Continued)

SRI International
ATTN: C. Hulbert

Stewart Radiance Lab
ATTN: R. Huppi

Technology International Corp
ATTN: W. Boquist

Teledyne Brown Engrg
ATTN: F. Leopard
ATTN: MS-12, Tech Library
ATTN: N. Passino

Toyon Research Corp
ATTN: J. Ise

Utah State University
ATTN: A. Steed
ATTN: C. Wyatt
ATTN: D. Baker
ATTN: K. Baker, Dir Atmos & Space Sci

Visidyne, Inc
ATTN: C. Humphrey
ATTN: H. Smith
ATTN: J. Carpenter
ATTN: T. Degges
ATTN: W. Reidy

Wayne State University
ATTN: R. Kummler

Wayne State University
ATTN: W. Kauppila

Spectral Sciences, Inc
ATTN: F. Bien